Sustained store-operated calcium entry utilizing activated chromatin state leads to instability in iTregs

Author

Huiyun Lyu[1,2#], Guohua Yuan[3,4#], Xinyi Liu[1,5], Xiaobo Wang[1,5], Shuang Geng[6], Tie Xia[1,5], Xuyu Zhou[7,8], Yinqing Li[3,4], Xiaoyu Hu[1,2,5], Yan Shi[1,2,5,6*]

Affiliations

[1]Institute for Immunology, Beijing Key Lab for Immunological Research on Chronic Diseases, Tsinghua University, 100084, Beijing, China.

[2]Tsinghua-Peking Center for Life Sciences, Tsinghua University, 100084, Beijing, China.

[3]IDG/McGovern Institute for Brain Research and School of Pharmaceutical Sciences, Tsinghua University, 100084, Beijing, China.

[4]MOE Key Laboratory of Bioinformatics, Center for Synthetic and Systems Biology, School of Pharmaceutical Sciences, Tsinghua University, Beijing, P. R. China.

[5]Department of Basic Medical Sciences, School of Medicine, Tsinghua University, 100084, Beijing, China.

[6]Department of Microbiology, Immunology and Infectious Diseases, Snyder Institute, University of Calgary, Calgary, Alberta, Canada.

[7]Key Laboratory of Pathogenic Microbiology and Immunology, Institute of Microbiology, Chinese Academy of Sciences, Beijing 100101, China.

[8]University of Chinese Academy of Sciences, Beijing 100049, China.

[#]These authors contributed equally

[*]Correspondence: Yan Shi, D301 Medical Sciences Bldg, Tsinghua University, 100084, Beijing, China
yanshiemail@mail.tsinghua.edu.cn

Abstract

Thymus-originated tTregs and *in vitro* induced iTregs are subsets of regulatory T cells. While they share the capacity of immune suppression, their stabilities are different, with iTregs losing their phenotype upon stimulation or under inflammatory milieu. Epigenetic differences, particularly methylation state of Foxp3 CNS2 region, provide an explanation for this shift. Whether additional regulations, including cellular signaling, could directly lead phenotypical instability requires further analysis. Here we show that upon TCR triggering, store-operated calcium entry (SOCE) and NFAT nuclear translocation are blunted in tTregs, yet fully operational in iTregs, similar to Tconvs. On the other hand, tTregs show minimal changes in their chromatin accessibility upon activation, in contrast to iTregs that demonstrate an activated chromatin state with highly accessible T cell activation and inflammation related genes. Assisted by several cofactors, NFAT driven by strong SOCE signaling in iTregs preferentially binds to primed opened T helper (T_H) genes, resulting in their activation normally observed only in Tconv activation, ultimately leads to instability. Conversely, suppression of SOCE in iTregs can partially rescue their phenotype. Thus our study adds two new layer, cellular signaling and chromatin accessibility, of understanding in Treg stability, and may provide a path for better clinical applications of Treg cell therapy.

Introduction

The regulatory T cells (Tregs) are key to maintain peripheral immune tolerance and to block excessive inflammatory reactions. There are two main populations of Tregs. The prototypical one originates from the thymus (tTreg), sharing a developmental program similar to conventional T cells [1,2]. Their TCRs are believed to have higher basal affinity to MHC, and express Foxp3 during CD4 single positive period [3]. The other population originates from the periphery (pTregs) via conversion of Tconvs, arising during inflammation with proper antigenic stimulation and inductive cytokine environment [4–6]. iTregs, mimicking the induction of pTregs, is a type of Tregs induced *in vitro* in the presence of TGF-β [7,8]. While iTregs share similarity in suppressive capacities to Tregs *in vivo* [9–11], they are different from tTregs in several aspects, particularly regarding their stabilities. Although tTregs in some occasions show certain levels of plasticity, their phenotypes are mostly stable, both *in vivo* and *in vitro* [12]. iTregs induced *in vitro* are more labile with marked loss of Foxp3 expression after activation, limiting the duration of their suppression [13,14]. The short life of iTregs is also a roadblocker of the clinical use of Treg cell therapy, as they cannot be used as an alternative source to replace numerically limited tTregs [15]; and in cases where iTregs are raised with targeted specificities, they carry concerns of potential self-reactivity following the loss of Foxp3.

The stability of tTregs is established prior to their exit from the thymus [16]. In the thymus, Foxp3 works with other transcription factors, such as NFAT and c-Rel to maintain a steady transcriptional program [17–19]. At the same time, the extensive demethylation of FoxP3 CNS2 is also critical to their stable phenotype, an event likely taking place before FoxP3 expression [19,20]. While epigenetic differences provide a possible explanation of Treg stability, it is more probable that multiple factors collectively contribute to the difference. Unlike Tconvs that undergo expansion, attrition and memory states after activation, tTregs lose signature changes and return to their original state following activation [21]. This persistence in phenotype of tTregs is certainly beneficial to the host, yet mechanisms for this maintenance, in contrast to the lack thereof in iTregs are incompletely understood. Previous work suggests that TCR signal as well as ensuing Ca^{2+} activities are weaker in tTregs [22–24], whether the reduced TCR signaling strength is the root of tTreg stability remains an intrigue, particularly strong TCR engagement facilitates iTregs' loss of phenotype.

Here we report a surprising finding that may contribute to the iTregs' phenotypical change after their activation. We found that ligation of TCR induces long vibration of Ca^{2+} signals in Tconvs that lasts for hours, as typically expected in the SOCE activation. Initially similar, this vibration is quickly diminished in tTregs, correlating with their reduced response to TCR stimulation. In contrast, in iTregs, this Ca^{2+} vibration is indistinguishable from Tconvs. The sustained Ca^{2+} signal leads to a strong NFAT activation in iTregs. Regarding chromatin accessibility, with the aid of our initial observation of iTregs

from the perspective of activated Tconv, we found iTregs also show an "activated" chromatin state with T cell activation and inflammation related genes highly open. We demonstrate that the NFAT nuclear translocation driven by sustained calcium signal allows its direct access to prime-opened T_H genes and upregulate their expression, destabilizing iTregs. As expected, blocking CRAC channel reverses the loss of FoxP3 in iTregs *in vitro* and *in vivo*. Our work therefore suggests that Ca^{2+} signaling and accessible chromatin state in iTregs are two key causes in their loss of stability following activation, which may be of important value to understand how these two populations of Tregs operate in the disease conditions and lead to better applications of iTregs in the clinic.

Results

iTregs use a suppression mechanism similar to that of tTregs

In our previous work, we found that Tregs show strong binding to DCs, which is a key mechanism for blocking DC's ability to engage other Tconvs [25]. The strong binding is due to low basal calcium oscillation of tTregs in the steady state [26], which leads to diminished mCalpain activation and commensurate reduced internalization of LFA-1. Furthermore, our previous study showed the low calcium oscillation is maintained by reduced expression of endosomal Ca^{2+} channel Ryr2 by Foxp3 [26]. To ascertain that this regulation is also central to iTregs, we produced iTregs from Tconvs. With plate bound anti-CD3/CD28 and in the presence of TGF-β, iTregs were induced and the percentage was maximized on day 2. We found that *in vitro* iTregs show stronger suppression than tTregs on OT-II proliferation in response to epitope peptide loaded DCs (Fig 1A). In accordance with the stronger suppression, single cell force spectroscopy analysis showed that iTregs possessed apparent binding to DCs, even stronger than tTregs (Fig 1B). In addition, iTregs also showed increased binding force compared with activated Tconvs (Fig 1C), suggesting the strong binding force is a common feature of both types of Tregs, but not Tconvs. We measured the expression of FoxP3 more precisely, and noticed that the protein level expression of FoxP3 reached its peak on day 2 after the induction (Fig 1D). With the accumulation of FoxP3 protein, basal Ca^{2+} oscillation in the treated Tconvs was gradually diminished, with the former leading the latter roughly by one day (Fig 1E). As expected, the transcription level of Ryr2 was suppressed both in iTregs and tTregs (Fig S1A), suggesting that the strong binding force with DC may come from reduced calcium oscillation as a result of FoxP3-mediated suppression of Ryr2 transcription. While Ryr2 expression may be regulated by Foxp3, the induction efficiency of Foxp3 was not affected by Ryr2 knock out (Fig S1B). Therefore, we show iTregs can apply a suppression mechanism similar to tTregs, which operates via the indirect inhibition via DC blockage. We do not know why iTregs show a stronger suppression than tTregs, an event maybe related to their activation in the induction process.

Sustainment of SOCE and NFAT nuclear translocation are reduced in tTregs, but not in iTregs

It was reported previously that TCR signaling led to a dramatic reduction of FoxP3+ cells in iTregs, but not in tTregs [14,27]. We reproduced this data in our lab (Fig 2A). tTregs have been reported to show an attenuated response to TCR triggering [22–24], the exact point of signal attenuation in tTregs has not been elucidated. In immune cells, there are mainly three types of Ca^{2+} signals, the steady state low level Ryr2-based membrane proximal Ca^{2+} "puff"; the TCR ligation-triggered, inositol triphosphate-mediated IP3R opening on the ER membrane; and ER Ca^{2+} depletion-induced, sustained Ca^{2+} influx upon SOCE activation [28]. As the extracellular Ca^{2+} is roughly 4 logs higher than the intracellular, SOCE activation is by far the strongest Ca^{2+} event in T cells (Fig S2A), and is also distinct from the other Ca^{2+} signaling patterns for its persistent vibration lasting hrs to days [29,30].

We wondered if the reported TCR signal truncation in tTregs was manifested as reduced SOCE activities. We titrated anti CD3/CD28 concentrations, and iTregs lost Foxp3 at the lowest dose required to activate, yet tTregs were resistant to an 8-fold increase in both (Fig S2B). To study the molecular basis for the weak response in tTregs, we first monitored the early SOCE intensity in iTregs and tTregs, we found the first wave of SOCE in iTregs was slightly higher than Tconvs and tTregs, but there was no discernable difference between tTregs and Tconvs (Fig 2B). In addition, the phosphorylation of CD3ζ was similar in Tconv and nTreg immediately after TCR crosslink (Fig S2C). As full T cell activation requires sustained SOCE activation [31], we extended the observation time window. As SOCE signal is synchronized upon initial TCR trigger, each individual T cell SOCE oscillation hours into activation is no longer in unison [29,32], we therefore recorded Ca^{2+} waves in individual cells. In Tconvs and iTregs, Ca^{2+} remained cyclic waves expected in SOCE pulsation. In contrast, this Ca^{2+} signal was suddenly lost in tTregs 40-50 min after the activation (Fig 2C) (Movie 1-3).

In contrast to other transcriptional factors, such as NF-κB, activated rapidly in response to short Ca^{2+} elevation, NFATs are known to be triggered only by sustained cytoplasmic Ca^{2+} [31,33,34]. Indeed, in contrast to iTregs and Tconvs, tTregs' NFATc1 and c2 failed to translocate into the nucleus (Fig 2D). Upon detailed analysis, in iTregs, anti-CD3/CD28 stimulation led a quick drop in cytoplasmic NFAT in two hours, with moderate accumulation of NFAT in the nucleus (Fig S2D). This was followed by continuous synthesis of NFAT in the cytoplasm and accumulation of nuclear NFAT [35,36]. While tTregs are known to have reduced NFAT activation in response to TCR ligation [22,37], our results pointed to a truncated Ca^{2+} response likely to be the molecular basis for this phenotype. With this association potentially established, we wondered if the length of SOCE itself is sufficient to explain the stability difference between iTregs and tTregs. Non-specific Ca^{2+} membrane permeability modifier such as

ionomycin resulted in large scale cell death (Fig S2E), we therefore used SERCA inhibitor Thapsigargin (TG). Blocking SERCA leads to endosome Ca^{2+} reloading blockage that leads to continuous translocation of STIMs to the plasma membrane-ER junction and Orai channel opening. In contrast to indiscriminating Ca^{2+} overload, pure SOCE activation was not followed by significant cell death (Fig S2E). As expected, some tTregs treated with TG lost their Foxp3 (Fig 3E). These results collectively argue that the truncated Ca^{2+} in tTregs is essential to protect tTregs from phenotypical shift.

iTregs display activated chromatin state with highly open activation region

As shown, the behaviors of SOCE signaling and NFAT of iTregs were closer to their precursor Tconvs rather than tTregs, we were curious about the systemic similarity among iTregs, Tconvs and tTregs. Therefore, we performed RNA-seq and Assay for Transposase-Accessible Chromatin with high-throughput sequencing (ATAC-seq) of iTregs, together with resting/activated tTregs and Tconvs.

In RNA-seq data, principal component analysis (PCA) and heatmap of DEG indicated that Tconvs were quite different before and after activation, but the changes of tTregs before and after TCR activation were more limited compared with Tconvs (Fig 3A and Fig S3C), verifying that tTregs have low TCR responsiveness. Comparing the transcriptome characteristics with other cell types, iTregs acquired partial Treg features after induction, shown as an intermediate between Tconvs and tTregs on PC2 (Fig 3A and Fig S3B). While among all cell states, iTregs had the highest PC1 scores, represents higher proliferation state, probably due to the 4 days of induction (Fig 3A and Fig S3A).

Next, we analyzed the chromatin accessibility of these cells using ATAC-seq data. In the PCA plot, tTregs showed fewer changes after activation compared to Tconvs, while iTregs were closer to activated Tconv cells (Fig 3C). In differential peak heatmap clustered by cell type, Tconvs became more accessible in “Activation Region” after activation, and with a dramatic increase in the overall accessibility (Fig 3C). However, the changes of tTregs after activation are limited, the majority of tTreg-specific accessible region, named “Treg Region”, were not changed. Also the activation region opening seen in Tconvs were not more accessible in tTregs (Fig 3C). All of these characteristics indicated that tTreg phenotype is highly ensured by their low TCR responsiveness which potentially led to their refusal to change chromatin accessibility seen in Tconvs following activation.

When comparing iTregs with the others, we found iTregs were highly accessible in activation region found in activated Tconvs (Fig 3C and Fig 3D). However, only a few Treg specific peaks shown in Treg region were opened in iTregs (Fig 3C and Fig 3E). For further analysis, we isolated Treg specific peaks. It was clear that most of them were opened in tTregs but showed little accessibility in

iTregs (Fig S3D). For example, Foxp3 and Ctla4, expressed in both tTregs and iTregs, show high accessibility in resting and activated tTregs, but were closed or only partially opened in iTregs (Fig 3G). In contrast, genes related to inflammation cytokine in T helper cells, such as Ifng, Il4, Il17ra and Il21, were highly opened in iTregs (Fig 3F). In further elaboration of Activation Region in Figure 3D, we have selected some genes including typical peaks that are within this region (Fig S3E). These genes encompass some T-cell activation-associated transcription factors, such as Irf4, Atf3, as well as multiple members of the Tnf family including Lta, Tnfsf4, Tnfsf8, and Tnfsf14. Additionally, genes related to inflammation cytokine and function such as Il12rb2, Il9, and Gzmc are included. These genes display elevated accessibility upon T-cell activation, partially open in activated tTreg cells. However, all of them exhibit high accessibility in iTreg cells.

Overall, we showed that at the gene expression level, iTregs have acquired some Treg features, but the chromatin accessibility was mostly trapped in activated Tconv state, not only with regard to the closed Treg genes, but also with genes associated with T activation and inflammation highly opened. The latter is expected to be mainly closed in genuine Tregs in accordance with their lower responsiveness to TCR triggering. We speculate that this “unconverted” chromatin accessibility, especially the highly opened activated genes will contribute to iTreg instability upon TCR stimulation. It is therefore interesting whether NFAT accumulated in nuclei driven by sustained calcium oscillation will indeed target those genes for an activation state unfit for their phenotypical stability.

SOCE and NFAT directly leads to phenotypical instability in iTregs

To further validate the role of calcium and NFAT in iTreg instability, we used inhibitors cyclosporine A (CsA) and CM-4620 to suppress calcium signal and NFAT, respectively. We found that inhibition of calcium or NFAT rescued the Foxp3 expression in iTregs upon restimulation (Fig 4A). Another SOCE inhibitor BTP2 was also verified (Fig S4A). Accordingly, ionomycin, which can directly induce calcium release independent of TCR activation, also lead to iTreg instability (Fig S4B). Thus, NFAT and calcium signaling blockage was correlated to iTreg stability. As control, inhibition of NFkB (BAY 11-7082), c-Jun (SP600125), or a c-Jun/c-Fos complex (T5224) had no discernable effect, or in one case, possibly further reduction in stability (Fig S4C). These results may indicate that NFAT plays a crucial and special role in TCR activation, which leads to iTreg instability.

To investigate how NFAT and calcium signaling destabilize iTregs, we performed RNA-seq on these cells. From the differential gene expression and principal component analysis, we found that iTregs upon restimulation showed significant differences from the resting state at the transcriptome level, and this difference could be substantially reduced with inhibition of calcium or NFAT (Fig 4B). As shown

in the PCA plot, calcium/NFAT-blocked iTregs were significantly closer to the resting state than the unstable ones (Fig 4C). Thus, inhibition of calcium or NFAT can significantly improve the stability of iTregs as reflected by transcriptomic identity. In addition, the large overlap (about 80%) of genes that were rescued by CM-4620 and by CsA further supported that calcium signaling change the fate of iTregs mainly through NFAT (Fig 4D).

Among the genes rescued by CM-4620 and CsA, they can be further divided into two groups. Members of the first group were downregulated upon restimulation and the downregulation was blocked by inhibition of calcium and NFAT. This result indicating that these genes are downregulated by NFAT. Among these genes, several of them are critical for functions and stability of Tregs, such as Foxp3, Id3, Il10rb, Sema4a, Tgfbr1/2, Ms4a4b, Nlrp6 (Fig 4B and Fig S4D). In the functional analysis of these genes, we found that Rap-1 pathway, PD-1/PD-L1 pathway and Foxo pathway were significantly enriched (Fig S4E). Loss of these genes was therefore consistent with the phenotype of iTreg instability.

The other group had genes that were otherwise upregulated after restimulation, but failed to do so with CM-4620 or CsA, indicating that these genes are upregulated by NFAT. In these genes, many of them are associated with T helper differentiation and T cell activation, such as Il21, Il12rb2, Tbx21, Gzma, Stat2, Stat3, Atf3, Fasl (Fig 4B and Fig 4F). Among them, Il21 encodes a key cytokine in Th17 differentiation, Tbx21, encoding T-bet, and Il12rb2 are key transcriptional factors and cytokine receptor for Th1 differentiation. Functional enrichment analysis of these upregulated genes pointed to Th17 related pathway and Th1/Th2 related pathways (Fig 4E). Further validation of these upregulation T helper related genes (T_H genes) by NFAT was perform by QPCR (Fig 4G). These results in all indicated the iTreg restimulation was associated with a strong tendency of differentiation towards non-Treg polarization, and NFAT was likely a key regulator in this process.

NFAT upregulate prime-opened T_H genes to destabilize iTregs

To further study the role of NFAT in iTreg instability, we performed Cut&Tag assay to acquire the NFAT binding sites in resting iTregs and those after restimulation (Fig 5A). NFAT-flag and anti-Flag antibody was used to capture peaks that were bound by NFAT (Fig S5A). The binding peaks were of high quality as indicated by the lower number of peaks in the mock control compared to both resting and activated states (Fig 5B). The number of NFAT peaks in restimulated iTregs was significantly higher than that in resting state, which was consistent with the massive nuclear translocation of NFAT indicated by western blot (Fig 5B and Fig 2D). For peak distribution at gene body, NFAT peaks both before and after restimulation were enriched at promoters/TSS and the first

introns of genes (Figures S5C).

For those upregulated T_H genes, we speculated that this may be associated with the highly "activated" chromatin state of iTregs mentioned earlier. Therefore, we first checked the chromatin accessibility around the transcription start site (TSS) in those genes and found that this group of genes was significantly more accessible in iTregs than in tTregs and Tconvs (Fig 5C). As shown in the genome browser view, Il21, Il12rb2 and Tbx21 were more open in iTregs, even more so than the activated Tconvs (Fig S5B). Further analysis revealed that NFAT significantly increased their binding to the TSS regions on upregulated Th genes after restimulation (Fig 5D), while showing little change on downregulated Treg genes (Fig 5SD). As shown by Il21, Tbx21 and Il12rb2, after activation, NFAT accumulated at the sites that were prime-opened resulting in their increased expression (Fig 5E). Therefore, the enhanced chromatin accessibility revealed in Fig 4 was indeed approached by the large amount of NFAT, leading to T cell polarization towards other directions with a sole reciprocal loss of polarization towards Tregs. This tendency may to some extent explain the rapid loss of iTreg phenotype.

As one potential counter argument, NFAT is ostensibly essential to the development of tTregs [38,39]. In the induction of iTregs, NFAT in collaboration with SMAD is also critical [23,39,40]. It is therefore intriguing why NFAT re-activation after iTreg formation may serve as a key factor in compromising iTreg stability. To resolve those seemingly contradictory regulations, we performed NFAT motif enrichment analysis. The results showed that putative BATF, AP-1(Fos/Jun), RORg binding sites were highly enriched in restimulation state specific regions (Fig 5F). For the preference of different co-factors to different gene subsets, SMAD family tended to bind to genes that were downregulated by NFAT, for example, Foxp3, while AP-1 and RORg preferred binding to genes that were upregulated by NFAT, such as T_H genes (Fig. 5G). Taken together, our results appear to suggest that upon restimulation of iTregs, NFAT prefers to cooperate with AP-1/RORg to promote the expression of prime opened T_H gene expression, and at the same time denies the SMAD programming that may be critical to maintain Treg functions and stabilities. Certainly, how much this selective cooperation between NFAT and other transcriptional factors contributes to iTreg instability remains speculative until large scale ChIP-seq analyses are performed on the players involved.

According to the Cut&Tag data, the secretion levels of IL-21 in tTreg and iTreg was also examined by ELISA. As shown in Fig 5H, tTreg did not secrete IL-21 regardless of activation status (undetectable), while iTreg did not secrete IL-21 at resting state but they did so after 48 h of restimulation. The secretion of IL-21 was inhibited by CsA and CM-4620 treatment. This observation aligns with our findings where nuclear binding of NFAT to gene loci of these cytokines enhanced their expression, pushing iTreg unstable under inflammatory conditions. These findings further underscore the

likelihood that the inhibition of calcium and NFAT signaling might contribute to the stabilization of iTreg by suppressing the secretion of inflammatory cytokines.

Reduction of SOCE enhances iTreg stability and suppressive potential

Given that sustained calcium signal and NFAT translocation can directly disrupt iTreg stability, we asked whether manipulation of calcium signaling or NFAT can conversely be used to stabilize those cells. As Treg suppression assays require the participation of other T cells which are sensitive to inhibitory agents added indiscriminately, after regular iTreg induction, we overexpressed a dominant negative ORAI (DN-ORAI), whose single monomer incorporation will lead to a functionally disabled ORAI hexamer, to control the SOCE signal upon iTreg restimulation [41]. As expected, the mutated ORAI reduced the SOCE signaling by about a half (Fig 6A). When we restimulated this DN-ORAI expressing iTregs with anti-CD3/CD28, they showed stronger stability with higher retention of Foxp3 than WT-ORAI iTregs (Fig 6B). Consistently, DN-ORAI iTregs displayed more potent suppressive activity than control iTreg in *in vitro* suppression assay (Fig 6C).

Finally, the stability of DN-ORAI iTregs *in vivo* was examined. In brief, OT-II iTregs were infected with DN-ORAI retrovirus and then purified by GFP fluorescence, then the $CD45.2^+$ GFP^+ Foxp3-RFP^+ iTregs were adoptively transferred into CD45.1 recipient, and OVA/Alum were administrated to restimulate DN-ORAI iTregs *in vivo*. Analysis of the percentage of $Foxp3^+$ cells in mLN 5 days after adoptive transfer showed that DN-ORAI iTregs were more resistant to the loss of Foxp3 and thus were more stable than control WT-ORAI iTregs (Fig 6D). These results collectively showed that weakened calcium signal and inhibition of NFAT can quantitatively prevent iTregs from losing more Foxp3 both *in vitro* and *in vivo*, thus permitting a stronger suppressive capacity and a longer stability.

Based on extensive opening of activation regions approached by NFAT in the process iTreg stimulation, we postulate that openness of activation region could be another crucial feature of Treg stability, in addition to closed Treg region by low TSDR. Beyond the basal regimens of anti-CD3, anti-CD28, IL-2, and TGF-β, several additional factors have been reported to enhance the stability of iTregs, including the use of retinoic acid, rapamycin, vitamin C, and AS2863619 as well as removal of CD28 signaling[42–46]. We observed if those new additions in some ways altered the state of TSDR as well as the the openness of activation region. Our findings revealed that Rapamycin and AS tended to close the activation region (Fig S6A), while Vc, removal of CD28, and AS increased the accessibility of Treg genes (Fig S6B). These results indicate that different treatments have varied impacts on the activation region and Treg region. Hence the selective and combinatorial use of those factors is an interesting proposal in the generation of more stable iTregs.

Discussion

tTregs are different from other subsets of CD4 T cells in the thymic determination of their phenotype. To some extent, this centric determination is closer to CD4/CD8 demarcation, rather than other polarizations in the peripheral environment [1,2]. The stable phenotype, even after activation, is critical to provide the baseline immune suppression [12]. pTregs/iTregs are driven by the environment. It is logical that those cells should be deprived of their suppressive ability when are no longer needed to avoid unnecessary accumulation of those cells. The current understanding is that during thymic development, FoxP3 CNS2 region is selectively demethylated, allowing several transcriptional factors, such as Ets1 and FoxP3 itself to binding to this location [19,20]. This is one of several epigenetic features that maintain the stability, and TCR signaling in tTregs does not change the pre-established hypomethylation state. Induced Tregs, on the other hand, use a different program that relies on the binding of SMADs to the CNS1 region to initiate FoxP3 expression [40]. This SMAD binding mediated transcription is dependent on Foxp3 H3K4me3 modification. In the absence of SMAD, H3K4me3 is partially lost, resulting in iTreg phenotypical shift [40]. Withstanding this paradigm, iTregs do not immediately lose FoxP3 expression upon TGF-β withdrawal, the loss of FoxP3 is evident hours or days after TCR signaling [27]. This indicates that while the epigenetic alterations are necessary, an activation event is required to drive the loss of phenotype. This notion is subtly echoed by the limited TCR signaling in tTregs, implying that the hypo responsiveness to TCR ligation may be a critical feature to maintain their stability.

We observed differences between tTregs and iTregs in calcium signal and Th gene accessibility. tTregs utilize both truncated calcium signal and conserved chromatin accessibility to systematically reduce their TCR responsiveness, ensuring their stability. In contrast, iTregs retain the full strength of the TCR signaling, particularly the sustained vibration of SOCE signal, the key factor that drives NFAT synthesis and nuclear translocation. With the help of several cofactors, such as AP-1, NFAT caused the high expression of these T_H genes, which subsequently subverts the original differentiation of iTregs, leading to their instability. Direct inhibition of SOCE signaling and NFAT can enhance iTreg stability *in vitro* and *in vivo* (Fig 6E).

Previous observations also showed that the calcium signal in tTreg is weaker than that in Tconvs, and NFAT activity is suppressed in tTregs. The weaker Ca^{2+} signal in previous reports was seen as early as 10 min into activation, this contradiction likely reflects the experimental settings and stimulation strength [24]. Nevertheless, in line with our results, inhibition of NFAT by low-dose CsA increased the number of tTreg in atopic dermatitis patients [47]. It seems reasonable to establish an inverse association between SOCE signal and Treg stability. In our analysis of the RNA-seq and

chromatin accessibility data, we did not identify any particular mechanism that may account for the distinct Ca^{2+} signal patterns in tTregs and iTregs. However, in contrast to Tconvs and iTregs, there must be a negative signal loop that blunts SOCE vibration in tTregs. We tried to sustain the calcium signaling in tTregs forcibly by thapsigargin, and indeed observed loss of Foxp3. However, as we at the moment cannot appreciate the finesse of this regulation, the underlying molecular details will require much more delicate approaches rather the brutal force of ER store depletion. In our view, future investigation in this direction may lead to better understanding of Treg biology as well as innovations in clinical Treg cell therapy.

Our results are consistent with the understanding that Treg-specific hypomethylation is crucial for tTregs to stably express their Treg-specific genes [19,20]. Those epigenetic changes are mostly absent in iTregs, resulting in their instability. The differences of accessibility in Treg genes were also observed in our ATAC-seq data. Therefore, current treatments such as Vitamin C and CD28 blockage applied to achieve demethylation and accessibility of Treg genes in iTregs are worthy attempts [44,45]. However, our work indicates that at least in ATAC-seq analyses, there are a cluster of activation and differentiation-related peaks present in iTregs that remain silent in tTregs upon TCR stimulation. Critically, these peaks were targeted by abundant NFAT in the iTreg nuclei following activation, leading to the upregulation of Th genes. This tendency of deviation away from Tregs may be another key player to iTreg instability. Our effort to produce highly stable iTregs would likely require a combined approach to demethylate Treg-specific genes and at the same time to block the activation and differentiation-related genes. In our work, targeting NFAT signaling during the restimulation phase appeared to be a potential method. Other ways that can directly close these genes will also likely be beneficial.

In this work, we stress the importance of NFAT signal in the instability of iTregs. Previous research has also unveiled the adverse effects of other TCR signaling pathways on Treg stability, such as NF-κB and mTOR. As all those factors may contribute to the shift in phenotype, it is out of scope of this report to directly compare all those factors. However, the value of this report is the identification of a key difference in Ca^{2+} signaling under TCR ligation that may explain the stability differences between iTregs and tTregs, which may open the door for additional regulations given the key role of SOCE activity in T cell activation.

Methods

Mice

All mice were in CD45.2 C57BL/6 background unless noted otherwise. OT-II-transgenic mice and CD45.1 mice were purchased from Jackson Laboratories. FoxP3-IRES-GFP transgenic mice (B6.Cg-Foxp3^{tm2Tch}/J, Strain #:006772 from Jackson Laboratory) were a gift from Dr. Hai Qi, School of Medicine, Tsinghua University. Foxp3-RFP mice were a gift from Dr. Xuyu Zhou, Institute of Microbiology, Chinese Academy of Sciences (CAS). Wild Type mice were purchased from Beijing Vital River Laboratory Animal Technology Co., Ltd. All mice were bred and housed at Tsinghua University Animal Facilities and maintained under specific pathogen-free conditions. All animal experiments were conducted in accordance of governmental and institutional guidelines for animal welfare and approved by the IACUC at the Tsinghua University.

Antibodies and Reagents

Recombinant Human IL-2 and human TGF-β were from R&D systems. Anti-mouse CD3 and biotin-anti-CD3 (145-2C11) mAb, anti-mouse CD28 and biotin-anti-CD28 (37.51) mAb, Purified Streptavidin were all from biolegend. LIVE/DEAD Fixable Aqua were from Invitrogen. For flow cytometric analysis, in addition to CD45.1 (A20) monoclonal antibody from Invitrogen, others were purchased from eBioscience or BD Pharmingen. The following clones were used: FoxP3(150D/E4), CD45.2 (104), CD4 (GK1.5), CD25 (PC61.5), CD44 (IM7), CD62L (MEL-14). Antibody used in immunoblot including NFATc1 Antibody (7A6) and NFATc2 Antibody (4G6-G5) were from Santa Cruz, Lamin A/C (4C11), β-Actin (13E5) and GAPDH (D4C6R) mAb were from CST. Monoclonal ANTI-FLAG® M2 antibody used in Cut&Tag assay was from Sigma. Mouse CD4 T Cell Isolation Kit used for the enrichment of $CD4^+$ T cells was from Stem cell. Foxp3/Transcription Factor Staining Buffer Set for Foxp3 staining was from eBioscience. NE-PER^{TM} Nuclear and Cytoplasmic Extraction Reagents used for immunoblot was from Thermo. All sequencing kit, including TruePrep DNA Library Prep Kit V2, Hyperactive Universal CUT&Tag Assay Kit and TruePrep Index Kit V2 was from Vazyme. For calcium mobilization, Ionomycin was from Beyotime and thapsigargin from Invitrogen. For inhibitors, cyclosporin A, CM-4620 and BTP2 were all from MCE. $OVA_{323-339}$ peptides from MBL. For Calcium imaging, Fluo-4 AM was from Thermo and Indo-1 AM from BD.

Flow Cytometry sorting and FACS

For surface marker detection, cells were incubated with Fc blocker (CD16/32 antibody; 2.4G2) for 5 min, and then incubated with surface antibody for 15 min at room temperature avoiding light. Foxp3 intracellular staining was performed by cell fixation and permeabilization using the Foxp3/

Transcription Factor Staining Buffer Set. Samples were analyzed on Fortessa cytometers (BD) with FACS Diva software and data were analyzed with Flowjo.

To prepare Tconv, tTreg and iTreg for experiments, spleen was isolated from 2-4-month-old Foxp3-GFP mice for Tconv and tTreg sorting, and 6-week-old mice for iTreg induction. Subsequently, CD4+ T cells were enriched using CD4 Isolation kit and stained with indicated surface markers. FACSAriaII (BD) was used for collecting particular population. The cell populations used are as follows: naive T cells, $CD4^+$ Foxp3-GFP^+ $CD44^{low}$ $CD62L^{high}$; tTreg cells, $CD4^+$ Foxp3-GFP^+; iTreg, Foxp3-RFP^+ or Foxp3-GFP^+. Infected iTreg, Foxp3-RFP^+ MSCV-GFP^+.

In vitro iTreg induction and Restimulation

$CD4^+$Foxp3-GFP^- $CD62L^{hi}CD44^{lo}$ (or Foxp3-RFP^-) naive T cells were sorted using 6-week-old mice and stimulated with plate-bound 0.5 μg/mL anti-CD3 and 1 μg/mL anti-CD28 in the presence of 2 ng/mL human TGF-β and 200 U/mL rhIL-2. iTreg was induced for 4d and sorted using Foxp3-GFP/RFP fluorescence, then cells were rested in fresh RPMI complete medium containing 200 U/mL rhIL2 for 1d.

For iTreg restimulation, iTreg was harvested plated at 0.4×10^6 cells for restimulation with plate-bound 0.5 μg/mL anti-CD3 and 1 μg/mL anti-CD28 in 96 plate. After 2d restimulation, Foxp3 was analyzed by intracellular staining.

Calcium Measurment

For Calcium influx within 10min upon TCR activation, sorted Foxp3-RFP^- Tconv, Foxp3-RFP^+ tTreg and Foxp3-GFP^+ iTreg were resting for 1d, then mixed and loaded with 1 μM Indo-1 AM at 37°C for 30 min in RPMI medium without FBS. Cells were then washed for twice in cold RPMI medium containing 1% FBS, followed by staining with biotinylated anti-CD3 and biotinylated anti-CD28 on ice for 1h. For calcium measurement, cells were heated in 37°C water bath for 5 min, then the baseline was recorded for 60 s on LSR II(BD). Calcium influx was triggered by the addition of 100μg/mL streptavidin to crosslink TCR. Data were analyzed using kenetics in FlowJo.

For calcium oscillation within 1h, Foxp3-RFP^- Tconv, Foxp3-RFP^+ tTreg, and Foxp3-RFP^+ iTreg were sorted and rested for 1d, then cells were loaded with Fluo-4 AM at 37°C for 30 min. After washing twice with PBS and further incubating in RPMI medium for 10min, cells were activated by plate-bound 0.5 μg/mL anti-CD3 and 1 μg/mL anti-CD28 in poly-L-lysine-coated confocal dish. Excess non-adherent cells were removed by flushing with buffer solution after 10 min. Fluorescence were recorded in the indicated time after stimulation as a time lapse for 20 min with an interval of 6 seconds. The mean fluorescence intensity changes over time in single cells were analyzed using

Surface in Imaris and normalized to resting fluorescence F0 (Fluo-4 F/F0), further the standard deviation of F/F0 in single cells was calculated and presented using GraphPad.

Immunoblot

iTreg, tTreg and Tconv were rested for 1d in RPMI medium containing rhIL-2 and treated with cyclosporine A (CsA) for 30 min before activated. Then these cells were stimulated by plate-bound 0.5 μg/mL anti-CD3 and 1 μg/mL anti-CD28 for indicated time, in the absence or presence of TGF-β. After stimulation, cells were immediately lysed using CERI, then nuclear and cytoplasmic component were separated using NE-PER^{TM} Nuclear and Cytoplasmic Extraction Reagents. After being mixed with SDS loading buffer and boiled for 10 min, the cytoplasmic and nuclear proteins equal to 5x10^5 iTreg and 2x10^{6} tTreg/Tconv were loaded onto 7.5% PAGE Gels. Then the protein was transferred onto a NC membrane and immunoblotted with NFATc1 and NFATc2, Actin and GAPDH were used as loading control of cytoplasmic protein, and LaminA/C as nuclear. Finally, the immunostained bands were detected by Super ECL Detection Reagent.

Treg cell suppression assay *in vitro*

10^4 purified DCs from splenocytes were pulsed with 2 μg/ml $OVA_{323-339}$ peptide, then iTreg and tTreg (2×10^4) were added onto DCs to occupy the latter for 30 min. $CD25^-$ OTII Tconv cells were sorted and stained by CFSE (Thermo Fisher Scientifc). 2×10^4 OTII Tconv cells were mixed in DC-Treg culture in a 96-well U bottom plate. The proliferation of OTII T cells was assessed after 2-4 d by CFSE dilution on flow cytometry.

DN-ORAI and NFAT-flag construction and Retrovirus infection

For DN-ORAI, ORAI CDS sequences were amplified from cDNA library and mutated with primer. Then WT-ORAI and DN-ORAI were linked with MSCV-GFP vector. For NFAT-Flag, Nfatc1-flag CDS was amplified from TetO-FUW-flag-Nfatc1 plasmid, and further linked with MSCV-GFP vector. For retrovirus production, platE cells were cultured with DMEM medium containing 10% FBS to 80%-90% confluence. For each 10cm dish, 10ug MSCV plasmid and 10ul Neofect transfection reagent were mixed in 500ul Opti-MEM medium. After 30 min incubation, the DNA mixture were added into the well and gently mixed. After 48 and 72 h, supernatant containing viruses was collected, filtered with 0.45um membrane. 8ug/mL polybrene was added to virus supernatant, then Foxp3-RFP+ iTreg was infected on the day 2 and 3 of induction by centrifugation at 1500g, 37°C 2h. On the day 5 of induction, the infected cells with GFP fluorescence and Foxp3-RFP iTreg was sorted and used.

In vivo iTreg stability

CD45.2^{+} Foxp3-RFP^{+} iTreg was sorted, and washed twice. 5X10$^{\wedge 6}$ cells were adoptively transferred into CD45.1 mice via tail vein. For DN-ORAI iTreg, CD45.2^{+} Foxp3-RFP^{+} iTreg was infected and GFP^{+}RFP^{+} iTreg was sorted to transfer to CD45.1 recipient. Six hours after cell transfer, mice were immunized with OVA protein mixed with Alum adjuvant in each hind flank. After 4 days of immunization, mLN were collected and the percentage of Foxp3+ cells in CD45.2^{+} was analyzed by intracellular staining.

AFM Based Single Cell Force Spectroscopy

The experiments were performed as previously described using a JPK CellHesion unit[25,48]. In brief, to measure Treg-DC adhesion forces in bicellular system, DC2.4 cells were cultured on untreated glass disks. iTreg/tTreg/Tconv cells were sorted and rested with rhIL2 overnight. The disks were moved into an AFM-compatible chamber and mounted on to the machine stage. The incubator chamber in which the machine was housed was conditioned at 37°C and at 5% CO2. A clean cantilever was coated with CellTak (BD), and then used to glue individual iTreg/tTreg/Tconv cells added to the disk. Only round and robust cells were selected for AFM gluing. The AFM cantilever carrying a single iTreg/tTreg/Tconv cell was lowered to allow T cell contact with an individual DC and to interact for 15 s before being moved upwards, until two cells were separated completely. The force curves were acquired. The process was then repeated. For each SCFS experiment, a pair of T–DC was used to generate force readings from each up and down cycle over a period of several minutes, a minimum of 14 force curves were collected in each T-DC pair. In all experiments, at least three such pairs were used for each condition. The force curves were further processed using the JPK image processing software.

RNA-seq

The RNA-seq library preparation was performed by a modified SMART-seq2 protocol[49,51]. Briefly, RNA was added into 4 µl elution mix made of 1 µl RT primer (10 µM), 1 µl dNTP mix (10 mM each), 1 µl RNase inhibitor (4 U/µl), and 1 µl H2O. Eluted samples were incubated at 72 °C for 3 min and immediately placed on ice. Each sample was added with 7 µl reverse transcription (RT) mix made of 0.75 µl H2O, 0.1 µl Maxima RNase-minus RT (Thermo Fisher Scientific, #EP0741), 2 µl 5x Maxima RT buffer, 2 µl Betaine (5 M, Sigma-Aldrich, B0300), 0.9 µl MgCl2 (100 mM), 1 µl TSO primer (10 µM), 0.25 µl RNase inhibitor (40 U/µl).The RT reaction was incubated at 42 °C for 90 min and followed by 10 cycles of (50 °C for 2 min, 42 °C for 2 min), then heat inactivated at 70 °C for 15 min. Samples were then amplified with an addition of 14 µl PCR mix made of 1 µl H2O, 0.5 µl ISPCR primer (10 µM), 12.5 µl KAPA HiFi HotStart ReadyMix (KAPA Biosystems, KK2602). The PCR

reaction was performed as follows: 98 °C for 3 min, 22 cycles of (98 °C for 15 sec, 67 °C for 20 sec, 72 °C for 6 min), and final extension at 72 °C for 5 min.

The amplified cDNA product was purified using VAHTS DNA Clean Beads. Sequencing libraries were prepared using TruePrep DNA Library Prep Kit V2 for Illumina (Vazyme, TD503-02).

Primer sequences: RT primer (Sangon), 5'Biotin-AAGCAGTGGTATCAACGCAGAGTACTTTTTTTTTTTTTTTTTTTTTTTTTTVN; TSO primer (Sangon), 5'Biotin-AAGCAGTGGTATCAACCAGAGTACAT/rG//rG//iXNA_G/; ISPCR primer (Sangon), 5'Biotin-AAGCAGTGGTATCAACGCAGA*G*T.

RNA-seq analysis

Raw fastq reads were trimmed by Cutadapt (version 1.18) to trim adapter and low quality sequence. Reads were aligned to the mouse genome (mm10) using STAR (version 2.5.3). The number of reads within each gene in each single cell were counted using RSEM (version 1.3.0) with gene annotation file from GENCODE (GRCm38.m23).

Differential expression was estimated by using DESeq2 package (version 1.26) with absolute log2 Fold change > 0.5 and adjusted P value < 0.05.

Functional enrichment analysis were performed by using the clusterProfiler R package (v3.14.3) with default parameters (P value < 0.05) and the functional annotations terms in Gene Ontology (GO)[50].

ATAC-sequencing

ATAC-seq were performed using TruePrep DNA Library Prep Kit V2 for Illumina according to the manufacturer's recommendation. Briefly, live cells were sorted using PI staining, then 5×10^4 cells were transferred to a low-binding centrifuge tube and resuspended in 50 μL of pre-chilled Lysis Buffer. After 20 times pipetting, cells were incubated on ice for 10 minutes for lysis. Subsequently, cells were pelleted by centrifugation at 4°C 500 g for 5 minutes, and suspended in a mixture consisting of 10 μL of 5× TTBL, 5 μL of TTE Mix V50, and 35 μL of ddH2O. The mixture was gently mixed by pipetting 20 times, and incubated at 37°C for 30 minutes for fragmentation. The products were purified using 2× VAHTS DNA Clean Beads, eluted with 26 μL of water, and collected for the subsequent amplification. 24 μl of the eluted samples were amplified with different combination of i7 index and i5 index primers. QPCR were performed to determine the cycle number for PCR amplification. 0.55×VAHTS DNA Clean Beads was employed for size selection of the PCR product. Finally, 30 ng of each sample were pooled for subsequent second-generation sequencing, on the Illumina NovaSeq 6000 with read length of 150 bp.

ATAC-seq analysis

Raw fastq reads were trimmed by Cutadapt (version 1.18) to trim adapter and low quality sequence. Reads were aligned to the mouse genome (mm10) using Bowtie2 (version 2.3.3.1), the parameters are -t -q -N 1 -L 25 -X 2000 --no-mixed --no-discordant. Reads with alignment quality < Q30, mapped to chrM, overlapping with ENCODE blacklisted regions) were discarded. Duplicates were removed using Picard (version 2.20.4) and Samtools (version 1.13). Open chromatin region peaks were called on using MACS2 peak caller (version 2.2.7.1) with the following parameters: -nomodel -nolambda -call-summits. Peaks from all samples were merged and peaks falls in ENCODE blacklisted regions were filtered out.

Differential peaks were estimated by using "edgeR" method in the R package DiffBind (version 2.14.0) with absolute log2 Fold change > 1 and adjusted P value < 0.05.

The peaks annotations were performed with the "annotatePeak" function in the R package ChIPseeker[52].

The plot of ATAC-seq signals over a set of genomic regions were calculated by using "computeMatrix" function in deepTools (version 2.0) and plotted by using "plotHeatmap" and "plotProfile" functions in deepTools.

Cut&Tag assay

Foxp3-RFP+ iTreg were induced, and infected with NFAT-Flag-GFP lentiviruses on day 1.5 and day 2.5 of induction. On day 5, Foxp3-RFP+ MSCV-NFAT-Flag-GFP+ iTregs were sorted, then rested and restimulated for 2 day. Cut&Tag assay were performed using Hyperactive Universal CUT&Tag Assay Kit for Illumina (Vazyme Biotech Co.,Ltd) according to the manufacturer's recommendation. Briefly, 1×10^5 iTregs were collected to low-binding centrifuge tubes and washed. Nucleus isolation were performed by NE buffer for 10 min on ice, and cross-linked by 0.1% formaldehyde for 2 min, then stopped by glycine. Con A Beads were pre-treated with binding buffer, and then incubated with nuclei of iTreg for 10 min. Further, samples were incubated with anti-Flag M2 antibody (1:50) or without primary antibody (Mock) overnight at 4°C. Goat Anti-Mouse IgG secondary antibody (1:50) was added and incubated for 1 h. Cells were washed three times, and then incubated with pA/G-Tnp enzyme for 1 h. After incubation, samples were mixed with 5×TTBL and Dig-300 Buffer and incubated at 37°C for 60 min for fragmentation. DNA was extracted and purified, then amplified with different combination of i7 index and i5 index primers. QPCR was performed to determine the cycle number for PCR amplification. VAHTS DNA Clean Beads were employed for size selection of the PCR product. Finally, 30 ng of each sample were pooled for subsequent second-generation sequencing,

584 on the Illumina NovaSeq 6000 with read length of 150 bp.
585
586 Cut&Tag data analysis
587 Raw fastq reads were trimmed by Cutadapt (version 1.18) to trim adapter and low quality sequence.
588 Reads were aligned to the mouse genome (mm10) using Bowtie2 (version 2.3.3.1), the parameters are
589 -t -q -N 1 -L 25 -X 2000 --no-mixed --no-discordant.
590 Reads with alignment quality < Q30, mapped to chrM, overlapping with ENCODE blacklisted regions
591 (https://sites.google.com/site/anshulkundaje/projects/blacklists) were discarded. Duplicates were
592 removed using Picard (version 2.20.4) and Samtools (version 1.13). Open chromatin region peaks
593 were called using MACS2 peak caller (version 2.2.7.1) with the following parameters: -nomodel
594 -nolambda -call-summits. Peaks from all samples were merged and peaks falls in ENCODE
595 blacklisted regions were filtered out.
596 The peaks annotations were performed with the "annotatePeak" function in the R package
597 ChIPseeker[52].
598 The plot of Cut&Tag signals over a set of genomic regions were calculated by using "computeMatrix"
599 function in deepTools and plotted by using "plotHeatmap" and "plotProfile" functions in deepTools.
600 The motif enrichment analysis was performed by using the "findMotifsGenome.pl" command in
601 HOMER with default parameters.
602 The motif occurrences in each peak were identified by using FIMO (MEME suite v5.0.4) with the
603 following settings: a first-order Markov background model, a P value cutoff of 10^{-4}, and PWMs from
604 the mouse HOCOMOCO motif database (v11).
605
606 Statistical analysis
607 Calculation and graphing were done with Prism (GraphPad). Data were presented as mean ± SEM,
608 unless indicated otherwise. Student's t test was used for comparing endpoint means of different groups.
609 P value < 0.05 was considered significant. *, P < 0.05; **, < 0.01; ***, < 0.001; ****, < 0.0001; N.S.,
610 not significant. Numbers of independently-performed experiment repeats are shown as N, biological
611 replicates of each experiment as n.
612
613
614

Acknowledgments

We thank Dr. Hai Qi for providing Foxp3-GFP mice, platE cell line and guidance of calcium-related experimental design. We thank Dr. Saiyong Zhu for providing TetO-FUW-flag-Nfatc1 plasmid. We also thank Imaging Core Facility, Technology Center for Protein Sciences of Tsinghua University for assistance. Y.S. is supported by the joint Peking-Tsinghua Center for Life Sciences, the National Natural Science Foundation of China General Program (31370878), State Key Program (31630023) and Innovative Research Group Program (81621002), by grants from CIHR (PJT-156334 and PJT-166155) and NSERC (RGPIN/03748-2018).

Author Contributions

H.L. performed all the experiments unless noted otherwise. G.Y. and H.L. perform RNA-seq experiment and all sequencing data analysis. X.L. performed AFM-related experiments. X.W. and S.G. provides suggestions to calcium-related expreiments and RNA-seq data analysis. T.X. provided biophysical mechanism on cell adhesion. X.Z. provided critical review on Treg biology. Y.L. provided critical technical support for sequencing experiment and data analysis. X.H. provided overall critical insight. Y.S. was responsible for the overall design and wrote the manuscript with inputs from X.H.

642 **Reference**

643 1. Rudensky, A.Y. (2011). Regulatory T cells and Foxp3. Immunological Reviews *241*, 260–268.
644 10.1111/j.1600-065X.2011.01018.x.
645 2. Sakaguchi, S., Yamaguchi, T., Nomura, T., and Ono, M. (2008). Regulatory T Cells and Immune
646 Tolerance. Cell *133*, 775–787. 10.1016/j.cell.2008.05.009.
647 3. Fontenot, J.D., Dooley, J.L., Farr, A.G., and Rudensky, A.Y. (2005). Developmental regulation of
648 Foxp3 expression during ontogeny. Journal of Experimental Medicine *202*, 901–906.
649 10.1084/jem.20050784.
650 4. Curotto de Lafaille, M.A., Lino, A.C., Kutchukhidze, N., and Lafaille, J.J. (2004). CD25− T Cells
651 Generate CD25+Foxp3+ Regulatory T Cells by Peripheral Expansion. The Journal of Immunology
652 *173*, 7259–7268. 10.4049/jimmunol.173.12.7259.
653 5. Apostolou, I., and von Boehmer, H. (2004). In Vivo Instruction of Suppressor Commitment in
654 Naive T Cells. Journal of Experimental Medicine *199*, 1401–1408. 10.1084/jem.20040249.
655 6. Cobbold, S.P., Castejon, R., Adams, E., Zelenika, D., Graca, L., Humm, S., and Waldmann, H.
656 (2004). Induction of *foxP3* + Regulatory T Cells in the Periphery of T Cell Receptor Transgenic Mice
657 Tolerized to Transplants. The Journal of Immunology *172*, 6003–6010.
658 10.4049/jimmunol.172.10.6003.
659 7. Chen, W., Jin, W., Hardegen, N., Lei, K., Li, L., Marinos, N., McGrady, G., and Wahl, S.M. (2003).
660 Conversion of Peripheral CD4+CD25- Naive T Cells to CD4+CD25+ Regulatory T Cells by TGF-beta
661 Induction of Transcription Factor Foxp3. Journal of Experimental Medicine *198*, 1875-1886.
662 10.1084/jem.20030152.
663 8. Fantini, M.C., Becker, C., Monteleone, G., Pallone, F., Galle, P.R., and Neurath, M.F. (2004).
664 Cutting Edge: TGF-β Induces a Regulatory Phenotype in CD4+CD25− T Cells through Foxp3
665 Induction and Down-Regulation of Smad7. The Journal of Immunology *172*, 5149–5153.
666 10.4049/jimmunol.172.9.5149.
667 9. Shevach, E.M., and Thornton, A.M. (2014). tTregs, pTregs, and iTregs: similarities and
668 differences. Immunol Rev *259*, 88–102. 10.1111/imr.12160.
669 10. Fu, S., Zhang, N., Yopp, A.C., Chen, D., Mao, M., Chen, D., Zhang, H., Ding, Y., and Bromberg,
670 J.S. (2004). TGF-beta Induces Foxp3 + T-Regulatory Cells from CD4 + CD25 - Precursors. Am J
671 Transplant *4*, 1614–1627. 10.1111/j.1600-6143.2004.00566.x.
672 11. Singh, A.K., Horvath, K.A., and Mohiuddin, M.M. (2009). Rapamycin Promotes the Enrichment
673 of CD4+CD25hiFoxP3+ T Regulatory Cells From Naïve CD4+ T Cells of Baboon That Suppress
674 Antiporcine Xenogenic Response In Vitro. Transplantation Proceedings *41*, 418–421.
675 10.1016/j.transproceed.2008.10.079.

12. Rubtsov, Y.P., Niec, R.E., Josefowicz, S., Li, L., Darce, J., Mathis, D., Benoist, C., and Rudensky, A.Y. (2010). Stability of the Regulatory T Cell Lineage in Vivo. Science *329*, 1667–1671. 10.1126/science.1191996.

13. Floess, S., Freyer, J., Siewert, C., Baron, U., Olek, S., Polansky, J., Schlawe, K., Chang, H.-D., Bopp, T., Schmitt, E., et al. (2007). Epigenetic Control of the foxp3 Locus in Regulatory T Cells. PLoS Biol *5*, e38. 10.1371/journal.pbio.0050038.

14. Chen, Q., Kim, Y.C., Laurence, A., Punkosdy, G.A., and Shevach, E.M. (2011). IL-2 Controls the Stability of Foxp3 Expression in TGF-β–Induced Foxp3 $^{+}$ T Cells In Vivo. J.I. *186*, 6329–6337. 10.4049/jimmunol.1100061.

15. Koenecke, C., Czeloth, N., Bubke, A., Schmitz, S., Kissenpfennig, A., Malissen, B., Huehn, J., Ganser, A., Förster, R., and Prinz, I. (2009). Alloantigen-specific *de novo*- induced Foxp3 $^{+}$ Treg revert *in vivo* and do not protect from experimental GVHD. Eur. J. Immunol. *39*, 3091–3096. 10.1002/eji.200939432.

16. Ohkura, N., Kitagawa, Y., and Sakaguchi, S. (2013). Development and Maintenance of Regulatory T cells. Immunity *38*, 414–423. 10.1016/j.immuni.2013.03.002.

17. Fu, W., Ergun, A., Lu, T., Hill, J.A., Haxhinasto, S., Fassett, M.S., Gazit, R., Adoro, S., Glimcher, L., Chan, S., et al. (2012). A multiply redundant genetic switch "locks in" the transcriptional signature of regulatory T cells. Nat Immunol *13*, 972–980. 10.1038/ni.2420.

18. Hill, J.A., Feuerer, M., Tash, K., Haxhinasto, S., Perez, J., Melamed, R., Mathis, D., and Benoist, C. (2007). Foxp3 Transcription-Factor-Dependent and -Independent Regulation of the Regulatory T Cell Transcriptional Signature. Immunity *27*, 786–800. 10.1016/j.immuni.2007.09.010.

19. Samstein, R.M., Arvey, A., Josefowicz, S.Z., Peng, X., Reynolds, A., Sandstrom, R., Neph, S., Sabo, P., Kim, J.M., Liao, W., et al. (2012). Foxp3 Exploits a Pre-Existent Enhancer Landscape for Regulatory T Cell Lineage Specification. Cell *151*, 153–166. 10.1016/j.cell.2012.06.053.

20. Ohkura, N., Hamaguchi, M., Morikawa, H., Sugimura, K., Tanaka, A., Ito, Y., Osaki, M., Tanaka, Y., Yamashita, R., Nakano, N., et al. (2012). T Cell Receptor Stimulation-Induced Epigenetic Changes and Foxp3 Expression Are Independent and Complementary Events Required for Treg Cell Development. Immunity *37*, 785–799. 10.1016/j.immuni.2012.09.010.

21. van der Veeken, J., Gonzalez, A.J., Cho, H., Arvey, A., Hemmers, S., Leslie, C.S., and Rudensky, A.Y. (2016). Memory of Inflammation in Regulatory T Cells. Cell *166*, 977–990. 10.1016/j.cell.2016.07.006.

22. Sumpter, T.L., Payne, K.K., and Wilkes, D.S. (2008). Regulation of the NFAT pathway discriminates CD4+CD25+ regulatory T cells from CD4+CD25– helper T cells. J Leukoc Biol *83*, 708-717. 10.1189/jlb.0507321

710 23. Vaeth, M., Schliesser, U., Muller, G., Reissig, S., Satoh, K., Tuettenberg, A., Jonuleit, H.,
711 Waisman, A., Muller, M.R., Serfling, E., et al. (2012). Dependence on nuclear factor of activated
712 T-cells (NFAT) levels discriminates conventional T cells from Foxp3+ regulatory T cells. Proceedings
713 of the National Academy of Sciences *109*, 16258–16263. 10.1073/pnas.1203870109.
714 24. Yan, D., Farache, J., Mingueneau, M., Mathis, D., and Benoist, C. (2015). Imbalanced signal
715 transduction in regulatory T cells expressing the transcription factor FoxP3. Proc Natl Acad Sci U S A
716 *112*, 14942-14947. 10.1073/pnas.1520393112
717 25. Chen, J., Ganguly, A., Mucsi, A.D., Meng, J., Yan, J., Detampel, P., Munro, F., Zhang, Z., Wu, M.,
718 Hari, A., et al. (2017). Strong adhesion by regulatory T cells induces dendritic cell cytoskeletal
719 polarization and contact-dependent lethargy. The Journal of Experimental Medicine *214*, 327–338.
720 10.1084/jem.20160620.
721 26. Wang, X., Geng, S., Meng, J., Kang, N., Liu, X., Xu, Y., Lv, H., Xu, Y., Xu, X., Song, X., et al.
722 (2022). FoxP3-mediated blockage of ryanodine receptor 2 is the molecular basis for the contact-based
723 suppression by regulatory T cells. BioRxiv. 10.1101/2022.05.02.490213.
724 27. Selvaraj, R.K., and Geiger, T.L. (2007). A Kinetic and Dynamic Analysis of Foxp3 Induced in T
725 Cells by TGF-β. J Immunol *178*, 7667–7677. 10.4049/jimmunol.178.12.7667.
726 28. Guse, A.H. (1998). Ca2+ signaling in T-Lymphocytes. Crit.Rev.Immuno *18*, 419–448.
727 10.1615/CritRevImmunol.v18.i5.20
728 29. Christo, S.N., Diener, K.R., and Hayball, J.D. (2015). The functional contribution of calcium ion
729 flux heterogeneity in T cells. Immunol Cell Biol *93*, 694–704. 10.1038/icb.2015.34.
730 30. Wülfing, C., Rabinowitz, J.D., Beeson, C., Sjaastad, M.D., McConnell, H.M., and Davis, M.M.
731 (1997). Kinetics and Extent of T Cell Activation as Measured with the Calcium Signal. Journal of
732 Experimental Medicine *185*, 1815–1825. 10.1084/jem.185.10.1815.
733 31. Dolmetsch, R.E., Xu, K., and Lewis, R.S. (1998). Calcium oscillations increase the efficiency and
734 specificity of gene expression. Nature *392*, 933-936. 10.1038/31960.
735 32. Le Borgne, M., Raju, S., Zinselmeyer, B.H., Le, V.T., Li, J., Wang, Y., Miller, M.J., and Shaw,
736 A.S. (2016). Real-Time Analysis of Calcium Signals during the Early Phase of T Cell Activation
737 Using a Genetically Encoded Calcium Biosensor. J.I. *196*, 1471–1479. 10.4049/jimmunol.1502414.
738 33. Dolmetsch, R.E., Lewis, R.S., and Goodnowt, C.C. (1997). Differential activation of transcription
739 factors induced by Ca2 + response amplitude and duration. Nature *386*, 855–858. 10.1038/386855a0
740 34. Tomida, T. (2003). NFAT functions as a working memory of Ca2+ signals in decoding Ca2+
741 oscillation. The EMBO Journal *22*, 3825–3832. 10.1093/emboj/cdg381.
742 35. Serfling, E., Chuvpilo, S., Liu, J., Höfer, T., and Palmetshofer, A. (2006). NFATc1 autoregulation:
743 a crucial step for cell-fate determination. Trends in Immunology *27*, 461–469.

744 10.1016/j.it.2006.08.005.
745 36. Zhou, B., Cron, R.Q., Wu, B., Genin, A., Wang, Z., Liu, S., Robson, P., and Baldwin, H.S. (2002).
746 Regulation of the Murine Nfatc1 Gene by NFATc2. Journal of Biological Chemistry *277*, 10704–
747 10711. 10.1074/jbc.M107068200.
748 37. Nayak, A., Glöckner-Pagel, J., Vaeth, M., Schumann, J.E., Buttmann, M., Bopp, T., Schmitt, E.,
749 Serfling, E., and Berberich-Siebelt, F. (2009). Sumoylation of the Transcription Factor NFATc1 Leads
750 to Its Subnuclear Relocalization and Interleukin-2 Repression by Histone Deacetylase. J. Biol. Chem.
751 *284*, 10935–10946. 10.1074/jbc.M900465200.
752 38. Li, X., Liang, Y., LeBlanc, M., Benner, C., and Zheng, Y. (2014). Function of a Foxp3 cis
753 -Element in Protecting Regulatory T Cell Identity. Cell *158*, 734–748. 10.1016/j.cell.2014.07.030.
754 39. Zheng, Y., Josefowicz, S., Chaudhry, A., Peng, X.P., Forbush, K., and Rudensky, A.Y. (2010).
755 Role of conserved non-coding DNA elements in the Foxp3 gene in regulatory T-cell fate. Nature *463*,
756 808–812. 10.1038/nature08750.
757 40. Tone, Y., Furuuchi, K., Kojima, Y., Tykocinski, M.L., Greene, M.I., and Tone, M. (2008). Smad3
758 and NFAT cooperate to induce Foxp3 expression through its enhancer. Nat Immunol *9*, 194–202.
759 10.1038/ni1549.
760 41. Mignen, O., Thompson, J.L., and Shuttleworth, T.J. (2008). Orai1 subunit stoichiometry of the
761 mammalian CRAC channel pore: CRAC channel subunit stoichiometry. The Journal of Physiology
762 *586*, 419–425. 10.1113/jphysiol.2007.147249.
763 42. Akamatsu, M., Mikami, N., Ohkura, N., Kawakami, R., Kitagawa, Y., Sugimoto, A., Hirota, K.,
764 Nakamura, N., Ujihara, S., Kurosaki, T., et al. (2019). Conversion of antigen-specific effector/memory
765 T cells into Foxp3-expressing T $_{reg}$ cells by inhibition of CDK8/19. Sci. Immunol. *4*, eaaw2707.
766 10.1126/sciimmunol.aaw2707.
767 43. Hill, J.A., Hall, J.A., Sun, C.-M., Cai, Q., Ghyselinck, N., Chambon, P., Belkaid, Y., Mathis, D.,
768 and Benoist, C. (2008). Retinoic Acid Enhances Foxp3 Induction Indirectly by Relieving Inhibition
769 from CD4+CD44hi Cells. Immunity *29*, 758–770. 10.1016/j.immuni.2008.09.018.
770 44. Mikami, N., Kawakami, R., Chen, K.Y., Sugimoto, A., Ohkura, N., and Sakaguchi, S. (2020).
771 Epigenetic conversion of conventional T cells into regulatory T cells by CD28 signal deprivation. Proc
772 Natl Acad Sci USA *117*, 12258–12268. 10.1073/pnas.1922600117.
773 45. Yue, X., Trifari, S., Äijö, T., Tsagaratou, A., Pastor, W.A., Zepeda-Martínez, J.A., Lio, C.-W.J.,
774 Li, X., Huang, Y., Vijayanand, P., et al. (2016). Control of Foxp3 stability through modulation of TET
775 activity. Journal of Experimental Medicine *213*, 377–397. 10.1084/jem.20151438.
776 46. Zhang, P., Tey, S.-K., Koyama, M., Kuns, R.D., Olver, S.D., Lineburg, K.E., Lor, M., Teal, B.E.,
777 Raffelt, N.C., Raju, J., et al. (2013). Induced Regulatory T Cells Promote Tolerance When Stabilized

778 by Rapamycin and IL-2 In Vivo. J.I. *191*, 5291–5303. 10.4049/jimmunol.1301181.
779 47. Brandt, C., Pavlovic, V., Radbruch, A., Worm, M., and Baumgrass, R. (2009). Low-dose
780 cyclosporine A therapy increases the regulatory T cell population in patients with atopic dermatitis.
781 Allergy *64*, 1588–1596. 10.1111/j.1398-9995.2009.02054.x.
782 48. Flach, T.L., Ng, G., Hari, A., Desrosiers, M.D., Zhang, P., Ward, S.M., Seamone, M.E., Vilaysane,
783 A., Mucsi, A.D., Fong, Y., et al. (2011). Alum interaction with dendritic cell membrane lipids is
784 essential for its adjuvanticity. Nat Med *17*, 479–487. 10.1038/nm.2306.
785 49. Habib, N., Li, Y., Heidenreich, M., Swiech, L., Avraham-Davidi, I., Trombetta, J.J., Hession, C.,
786 Zhang, F., and Regev, A. (2016). Div-Seq: Single-nucleus RNA-Seq reveals dynamics of rare adult
787 newborn neurons. Science *353*, 925–928. 10.1126/science.aad7038.
788 50. Ashburner, M., Ball, C.A., Blake, J.A., Botstein, D., Butler, H., Cherry, J.M., Davis, A.P.,
789 Dolinski, K., Dwight, S.S., Eppig, J.T., et al. (2000). Gene Ontology: tool for the unification of biology.
790 Nat Genet *25*, 25–29. 10.1038/75556.
791 51. Picelli, S., Faridani, O.R., Björklund, Å.K., Winberg, G., Sagasser, S., and Sandberg, R. (2014).
792 Full-length RNA-seq from single cells using Smart-seq2. Nat Protoc *9*, 171–181.
793 10.1038/nprot.2014.006.
794 52. Yu, G., Wang, L.-G., and He, Q.-Y. (2015). ChIPseeker: an R/Bioconductor package for ChIP
795 peak annotation, comparison and visualization. Bioinformatics *31*, 2382–2383.
796 10.1093/bioinformatics/btv145.
797
798
799
800
801
802
803
804
805
806
807
808
809
810
811
812

Figures

Fig 1. iTreg share similar suppressive mechanism to tTregs

A. Comparison of suppressive activity between tTreg and iTreg. CFSE-labelled OT-II T cells were stimulated with OVA-pulsed DC, then Foxp3-GFP^{+} iTregs and tTregs were added to the culture to suppress the OT-II proliferation. After 4 days, CFSE dilution were analyzed. n=3, N=3. Left, Representative histograms of CFSE in divided Tconvs. Right, graph for the percentage of divided Tconvs.

B. iTregs possessed stronger binding force to DCs than tTreg. A schematic diagram for AFM-SCFS assay setup (left). SCFS force readings for Tconv, tTreg and iTreg adhering to DC2.4 cells, one line represents a pair of T-DC, every dot represents force reading from each contact. Mean force of Tconv, tTreg and iTregs adhering to DC2.4 cells.

C. iTregs showed increased binding force compared with activated Tconvs. Mean force of Tconv, activated Tconv and iTreg adhering to DC2.4 cells. n>45, N=3.

D. Precise expression of FoxP3 was assessed during iTreg induction. Naïve Tconvs were stimulated with anti-CD3 and anti-CD28, in the presence of TGF-β and IL2 to induce iTregs. Cells were harvested at the indicated time and Foxp3 expression was analyzed by intracellular staining.

E. Basal Ca^{2+} oscillation was assessed during iTreg induction. Naïve Tconvs were stimulated with anti-CD3 and anti-CD28, in the presence of TGF-β and IL2 to induce iTregs. Cells were harvested at the indicated time and loaded with Fluo-4 AM, and Fluo-4 fluorescence over time were recorded with confocal microscope. The change of intracellular free Ca^{2+} concentration over time were shown as F/F0. The ratio of oscillated cells and standard deviation of F/F0 were calculated. n>150, N=3.

Here, **, $P < 0.01$; ***, $P < 0.001$; ****, $P < 0.0001$, by students's t test.

Fig 2. Diminished SOCE signal and NFAT translocation in tTregs, but not in iTregs

A. Comparison of Treg stability between tTregs and iTregs. iTregs and tTregs were sorted and restimulated with anti-CD3 and anti-CD28 antibodies. Cells were harvested after 2 d restimulation and Foxp3 expression was analyzed by intracellular staining. The percentages of $Foxp3^+$ cells were monitored by FACS. Left, representative histograms of restimulated iTregs. Right, graph for the percentage of $Foxp3^+$ cells in all $CD4^+$ cells. n=4, N=5.

B. Early SOCE signal was measured in iTreg, tTreg and Tconv by flow cytometry. Sorted Foxp3-RFP^+ iTreg and Foxp3-GFP^+ tTreg and double negative Tconv cells were mixed and loaded with Indo-1 AM, then stained with biotin-anti-CD3 and biotin anti-CD28 for 1 h, the base line fluorescence was recorded for 1 min, and then TCR crosslink was perform by the addition of streptavidin. Left, the gate of three mixed cells. Right, Indo-1 AM ratio of these cells upon TCR crosslink. N=3.

C. Long term SOCE were truncated in tTreg, but sustained in iTreg. Tconv, tTreg, and iTreg cells were loaded with Fluo-4 AM and activated by anti-CD3 and anti-CD28 in confocal dish. Fluorescence was recorded in the indicated time after stimulation with the interval of 10 s. Left, the F/F0 of mean fluorescence intensities were calculated and presented, Right, graph for standard deviation of fluorescence in these cells. n>50, N=3.

D. NFAT accumulate much in nucleus of iTreg, but not in tTreg. Tconv, tTreg, and iTreg cells were stimulated by anti-CD3 and anti-CD28, after the indicated times, cells were lysed and the cytoplasmic/nuclear components were separated. The cytoplasmic and nuclear NFATc1 and NFATc2 were analyzed by western blot. Actin and GAPDH were used as loading control of cytoplasmic proteins, and LaminA/C as nuclear. N=4.

E. Forcibly sustained calcium signal destabilizes tTreg. Foxp3-RFP^+ tTregs were stimulated by anti-CD3 and anti-CD28. After 1 h, various concentrations TG were added in the culture medium. Cells were collected after 24 h stimulation and Foxp3 expression was analyzed by intracellular staining. Left, representative histograms of treated tTregs. Right, graph for the percentage of $Foxp3^+$ cells in all tTregs. n=3, N=3.

Here, *, $P < 0.05$; **, $P < 0.01$; ***, $P < 0.001$; ****, $P < 0.0001$, by students's t test.

Fig 3. iTregs display highly open chromatin state at the activation and differentiation-related genes

A. PCA visualization of transcriptional profiles of Tconvs, tTregs and iTregs with or without TCR stimulation. Color indicates cell types.

B. PCA visualization of chromatin accessibility profiles of different cell types. Color indicates cell type.

C. Heatmap showing the chromatin accessibility of cell type specifically accessible peaks. As shown, two major groups of genes were labelled on right.

D. Line plots (top) and heatmaps (bottom) of activation regions in Tconvs, iTregs and tTregs. Activation regions were determined by a threshold of adjusted $P<0.05$ calculated by DESeq2.

E. Line plots (top) and heatmaps (bottom) of Treg regions in Tconvs, iTregs and tTregs. Treg regions were determined by a threshold of adjusted $P<0.05$ calculated by DESeq2.

F. Genomic track showing the chromatin accessibility of Ifng, Il4, Il17ra, Il21.

G. Genomic track showing the chromatin accessibility of Foxp3, Ctla4.

Fig 4. SOCE signaling and NFAT can disrupt iTreg stability

A. Impact of calcium signal and NFAT on iTreg stability. Sorted Foxp3-GFP$^+$ iTregs were rested for 1d, then restimulated by anti-CD3 and CD28 in the presence of CsA and CM-4620. Percentages of Foxp3$^+$ cells were analyzed by intracellular staining after 2d restimulation. Left, representative histograms of CsA and CM-4620-treated iTregs. Right, graph for the percentages of CsA and CM-4620-treated Foxp3$^+$ cells in all CD4$^+$ cells. n=4, N=8.

B. Heatmap showing the decreased changes for restimulated iTregs with CM-4620 or CsA. Typical genes were highlighted.

C. PCA visualization of transcriptional profiles of iTregs at different states. Color indicates cell states.

D. Venn plot showing the overlap of DEGs rescued by adding CM-4620 or CsA.

E. Biological terms enriched by the significant upregulated genes after iTreg restimulation rescued by inhibiting Calcium or NFAT.

F. Representative genes upregulated after iTreg restimulation rescued by inhibiting Calcium or NFAT.

G. QPCR of Foxp3 and Th-differentiated gene expression in the resting, restimulated and CsA/CM-4620-treated iTregs.

Here, *, $P < 0.05$; **， $p<0.01$, by students's t test.

Fig 5. NFAT disrupt iTreg stability by upregulating prime opened T_H genes

A. Model of CUT&Tag experiments to capture the binding sites of NFATc1.

B. The number of NFAT Cut&Tag peaks in mock control, resting iTregs, and restimulated iTregs.

C. Normalized counts of ATAC-seq reads in resting and activated Tconvs, resting and activated tTregs and iTregs, centered on the TSS region of NFAT-upregulated T_H genes.

D. Normalized counts of NFAT Cut&Tag reads in resting and restimulated iTreg, centered on the TSS region NFAT-upregulated T_H genes.

E. Genome track visualization of NFAT binding profiles and chromatin accessibility profiles in typical genes Il21, Il12rb2, and Tbx21.

F. Motif enriched in peaks with higher NFAT Cut&Tag signals in restimulated iTreg versus resting iTreg. List of five representative motifs ranked based on the p-values. The enrichment was performed by using HOMER.

G. The enrichment of motif occurrence for typical NFAT co-factors Smad, Fos/Jun, Rorc in the NFAT peaks in NFAT-upregulated or NFAT-downregulated genes after restimulation. P-value was from fisher's exact test.

H. IL-21 secretion in tTreg and iTreg upon activation. iTregs and tTregs were sorted and restimulated with anti-CD3 and anti-CD28 antibodies, in the presence of CsA and CM-4620. Cell culture supernatants were harvested after 2 d restimulation and IL-21 secretion was analyzed by ELISA. n=3.

Fig 6. Manipulation of SOCE can enhance iTreg stability

A. Manipulation of SOCE signal by dominant negative ORAI (DN-ORAI). SOCE was recorded in DN-ORAI iTreg cells loaded with Fura-Red by flow cytometry, TG was added after 1 min to induce ER depletion, 5 mins later 2 mM calcium was added to induce calcium influx. N=3.

B. Stability of iTreg was enhanced by DN-ORAI. iTregs were infected with WT-ORAI and DN-ORAI, and then restimulated by anti-CD3 and CD28 for 2 d. Percentages of Foxp3 were analyzed by intracellular staining. Left, representative histograms of Foxp3 expression in DN-ORAI iTregs. Right, graph for the percentages of $Foxp3^+$ cells in all CD4+ cells. n=3, N=3.

C. DN-ORAI enhances iTreg suppressive capacity. CFSE-labelled OT-II T cells were stimulated with OVA-pulsed DC, Foxp3-GFP^+ WT-ORAI/DN-ORAI iTregs were added to the culture to suppress the OT-II proliferation. After 40 hours, CFSE dilutions were analyzed. n=3, N=3.

D. Stability of DN-ORAI iTreg *in vivo*. WT-ORAI/DN-ORAI-GFP^+-transfected $CD45.2^+$ Foxp3-RFP^+ OT-II iTregs were transferred i.v. into CD45.1 mice. Recipients were immunized with OVA323-339 in Alum adjuvant. On day 5, mLN and spleen were harvested and analyzed for Foxp3 expression by intracellular staining. Up, Schematic representation of adoptive transfer experiment. Bottom right, histograms of Foxp3 expression in $CD4^+CD45.1^+$cells in spleen and mLN; Bottom left, graph for the percentages of $Foxp3^+$ cells in all $CD45.2^+$ cells in mLN. n=3, N=3.

E. Proposed model. The diminished calcium signal and closed chromatin structure in tTregs protect them from genetic and epigenetic disturbances, and the sustained calcium signal in iTregs cause NFAT aggregation in the nucleus, which makes use of a pre-opened gene loci to upregulate T_H genes, thus resulting the instability of iTregs.

Here, *, $P < 0.05$; **, $P < 0.01$; ****, $P < 0.0001$, by students's t test.

Supplementary Figures

Fig S1. Expression of Ryr2 in iTreg and the effect of Ryr2 on iTreg induction

A. QPCR for Ryr2 mRNA expression in iTregs, tTregs and Tconvs. n=3, N=4.

B. The effect of Ryr2 expression on iTreg induction. Naïve Tconv cells were sorted from Ryr2 fl/fl; CD4 cre mice and control Ryr2 fl/fl mice, then cells were differentiated into iTregs for 4 d. The percentages of $Foxp3^+$ cells were analyzed by intracellular staining after 4 d induction. Left, representative histograms of induced iTregs. Right, graph for the percentage of $Foxp3^+$ cells in all $CD4^+$ cells. n=3, N=3.

Here, ***, $P < 0.001$, by students's t test.

Fig S2. TCR responsiveness and NFAT translocation in tTregs and iTregs

A. Calcium oscillation were recorded in steady state and after anti-CD3 and anti-CD28 activation. Tconv cells were loaded with Fluo-4 AM, and left in steady state without anti-CD3 and anti-CD28 stimulation, or treated with anti-CD3 and anti-CD28 stimulation to record SOCE signal. Fluorescence was recorded with the interval of 10 s. Left, the F/F0 of mean fluorescence intensities were calculated and presented, Right, graph for standard deviation of fluorescence in these cells. n>50, N=3.

B. tTreg and iTreg cells was sorted and restimulated with various concentrations of anti-CD3 and anti-CD28 antibodies. The percentage of $Foxp3^+$ cells was analyzed by intracellular staining after 2d restimulation. n=3, N=3.

C. Early TCR signal of pCD3ζ in tTreg and iTreg after TCR cross-linking. Sorted iTreg, tTreg and Tconv cells were mixed and stained with biotin-anti-CD3 and biotin anti-CD28 for 1 h. TCR crosslink was perform by the addition of streptavidin. Cells were fixed at the indicated times and stained with pCD3ζ Y142 antibody. Left, representative flow overlays for pCD3ζ Y142 in rest and activated cells. Right, graph for the MFI changes in activated cells after indicated time.

D. Foxp3-RFP^+ iTreg were stimulated by anti-CD3 and anti-CD28, after the indicated times, cells were collected and the cytoplasmic/Nuclear component were separated. The cytoplasmic and nuclear NFATc1 and NFATc2 were analyzed by western blot. Actin and GAPDH were used as loading control of cytoplasmic protein, and Lamin A/C as nuclear. N=3.

E. Foxp3-RFP^+ tTregs were stimulated by anti-CD3 and anti-CD28, after 1h ionomycin and TG were added in the culture medium. After 24h of stimulation, the percentages of live cells in $CD4^+$ cells were monitored. N=3.

Here, **, $P < 0.01$, by students's t test.

Fig S3. iTreg has highest proliferation state and partial Treg feature

A. Left, heatmap showing the top genes that positively contribute to PC1. Right, heatmap showing the top genes that negatively contribute to PC1. As shown, genes contributing positively to PC1 mainly belong to proliferation such as nuclear division, DNA replication and cell cycle, while the negatively associated ones mainly belong to chromatin state regulations such as histone/DNA modification.

B. Left, heatmap showing the top genes that positively contribute to PC2. Right, heatmap showing the top genes that negatively contribute to PC2. As shown, the main contributors to PC2 axis were the signature genes of Tconvs and Tregs, such as Ifng, Il17ra, T-bet in the positive direction, Foxp3, Ctla4, Tnfrsf9 in the negative direction.

C. Heatmap showing the expression of cell type specifically expressed genes in RNA-Seq data. As shown, four major groups of genes were identified, based on the significant higher expression in specific cell types. Different group of genes were labeled.

D. Heatmap showing the chromatin accessibility of tTreg specifically accessible peaks in tTreg specifically expressed genes.

E. Genomic track showing chromatin accessibility of Irf4, Atf3, Lta, Tnfsf8, Tnfsf4, Tnsfsf14, Il12rb2, Il9, Gzmc in activated Tconv and iTreg.

Fig S4. SOCE signaling and NFAT cause instability and downregulate Treg related gene

A. Stability of iTreg treated with CM-4620, CsA and BTP-2 upon restimulation. iTregs were restimulated by anti-CD3 and CD28 in the presence of CsA, CM-4620 and BTP-2. Percentages of Foxp3+ cells were analyzed by intracellular staining after 2 d restimulation. Left, representative histograms. Right, graph for the percentages of Foxp3. n=3, N=3.

B. Stability of ionomycin and CsA treated iTreg. iTreg were treated with ionomycin and CsA, percentages of Foxp3+ cells were analyzed by intracellular staining after 1 d restimulation. n=3, N=3.

C. Stability of NF-kb and c-Jun/c-Fos inhibitor treated iTreg. Sorted Foxp3-GFP+ iTregs were rested for 1d, then restimulated by anti-CD3 and CD28 in the presence of indicated inhibitors. Percentages of Foxp3+ cells were analyzed by intracellular staining after 2d restimulation. n=3.

D. Representative genes downregulated after iTreg restimulation rescued by inhibiting Calcium or NFAT.

E. Biological terms enriched by the significant downregulated genes after iTreg restimulation rescued by inhibiting Calcium or NFAT.

Here, *, $P < 0.05$; **, $P < 0.01$, ***, $P < 0.001$, ****, $P < 0.0001$, by students's t test.

Fig S5. iTregs have highest accessibility in T_H-associated genes

A. Sorted Foxp3-RFP$^+$ naïve Tconvs were induced into iTregs in the presence of IL-2 and TGF-β for 4 days, on the second day and third day, iTreg cells were infected with retrovirus packaging with NFAT-flag plasmid. The infected Foxp3-RFP$^+$ iTregs were sorted and restimulated by anti-CD3 and CD28 for 1d. after 1d stimulation, the cells were collected and performed Cut&Tag assay.
B. Genome track visualization of chromatin accessibility profiles in typical genes Il21, Il12rb2, and Tbx21.
C. The genomic distribution of Cut&Tag peaks for NFAT in rest iTregs and restimulated iTregs.
D. Normalized counts of NFAT Cut&Tag reads in resting and restimulated iTreg, centered on the TSS region NFAT-downregulated Treg genes.

Fig S6. Different optimization of iTreg have various impact on activation region and Treg region

A. Line plots (top) and heatmaps (bottom) of activation regions in anti-CD3, anti-CD28, IL-2 and TGF-β induced iTregs, treated with Retinoic acid, Rapamycin, Vitamin C, removal of CD28, and AS2863619.
B. Line plots (top) and heatmaps (bottom) of Treg regions in anti-CD3, anti-CD28, IL-2 and TGF-β induced iTregs, treated with Retinoic acid, Rapamycin, Vitamin C, removal of CD28, and AS2863619.

Movie 1-3. Imaging of SOCE signal in Tconvs, tTregs and iTregs.

Tconvs (Movie 1), tTregs (Movie 2) and iTregs (Movie 3) were sorted and resting for 1d, then cells were loaded with Fluo-4 AM and activated by anti-CD3 and anti-CD28 in confocal dish. After activation for 50 min, movies were recorded for total 600 s with the interval of 10 s.

Figure 1

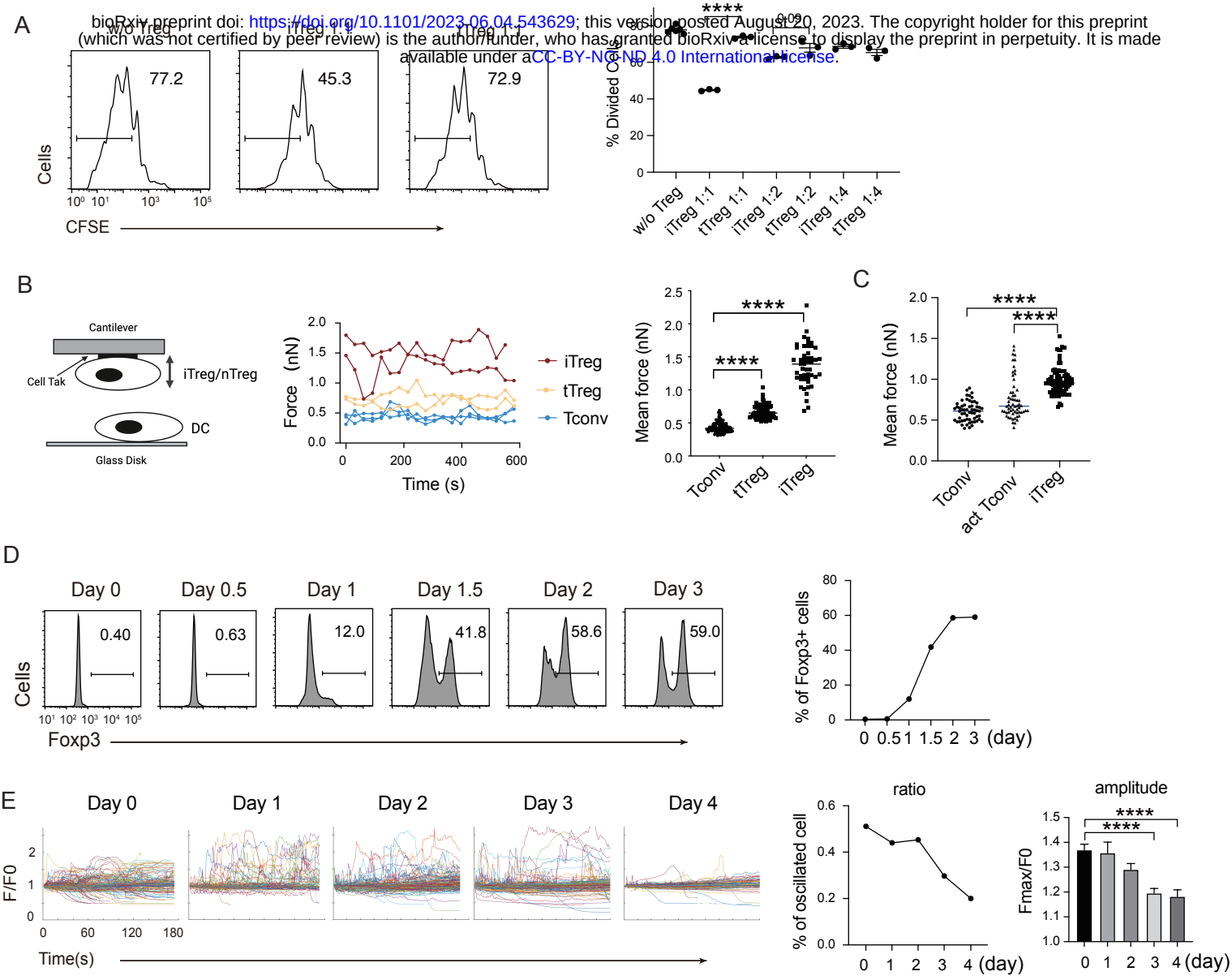

Figure 2

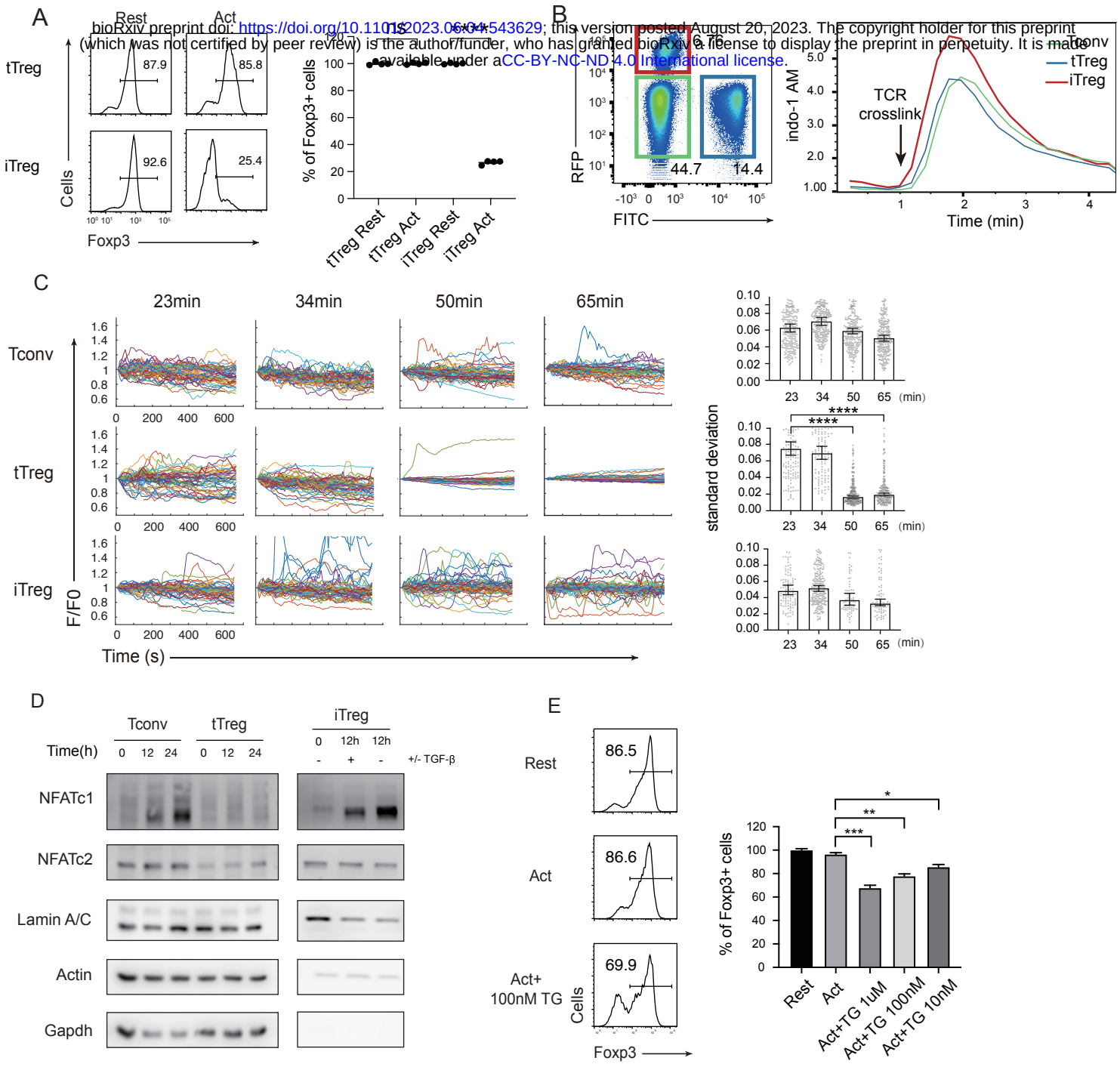

Figure 3

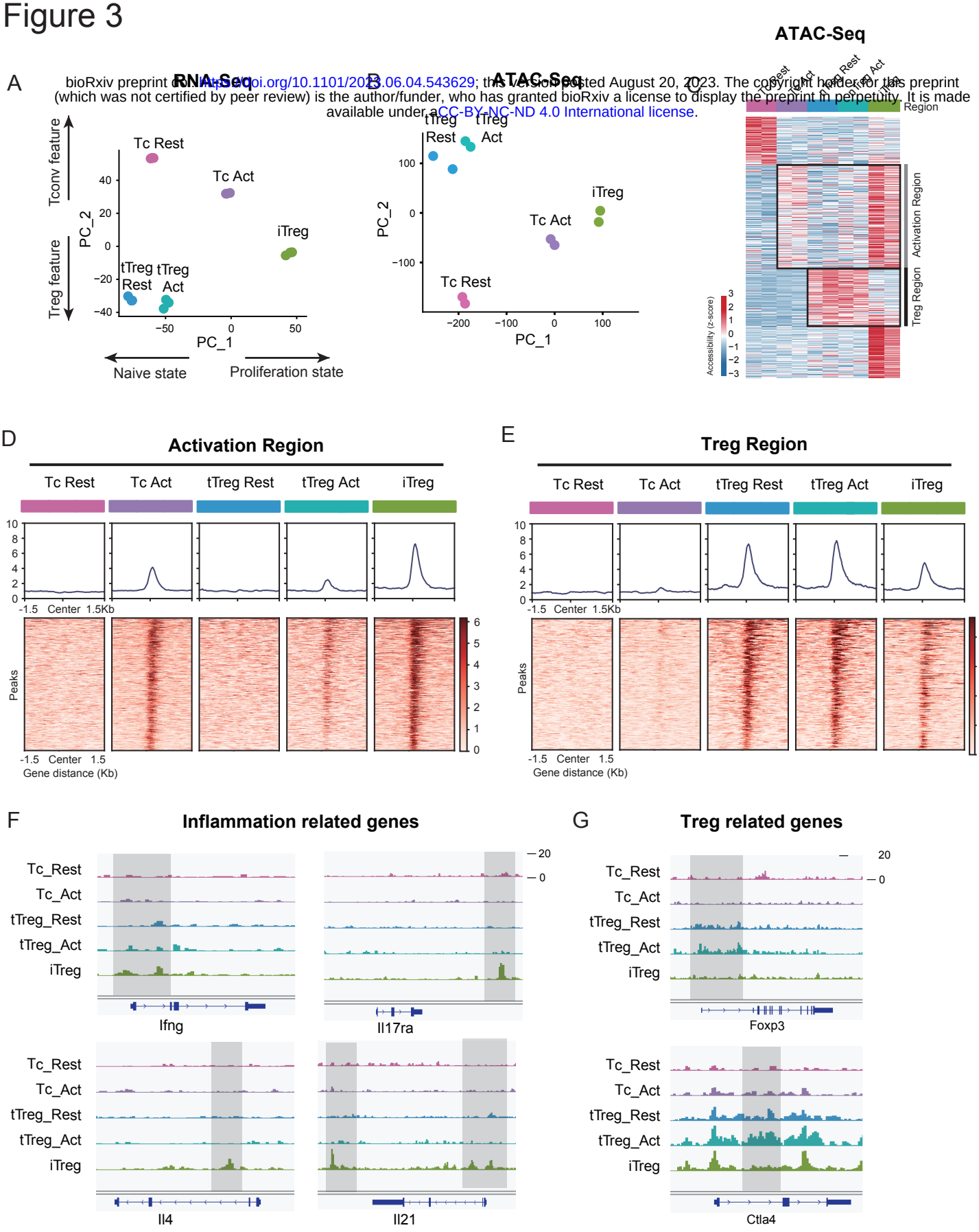

Figure 4

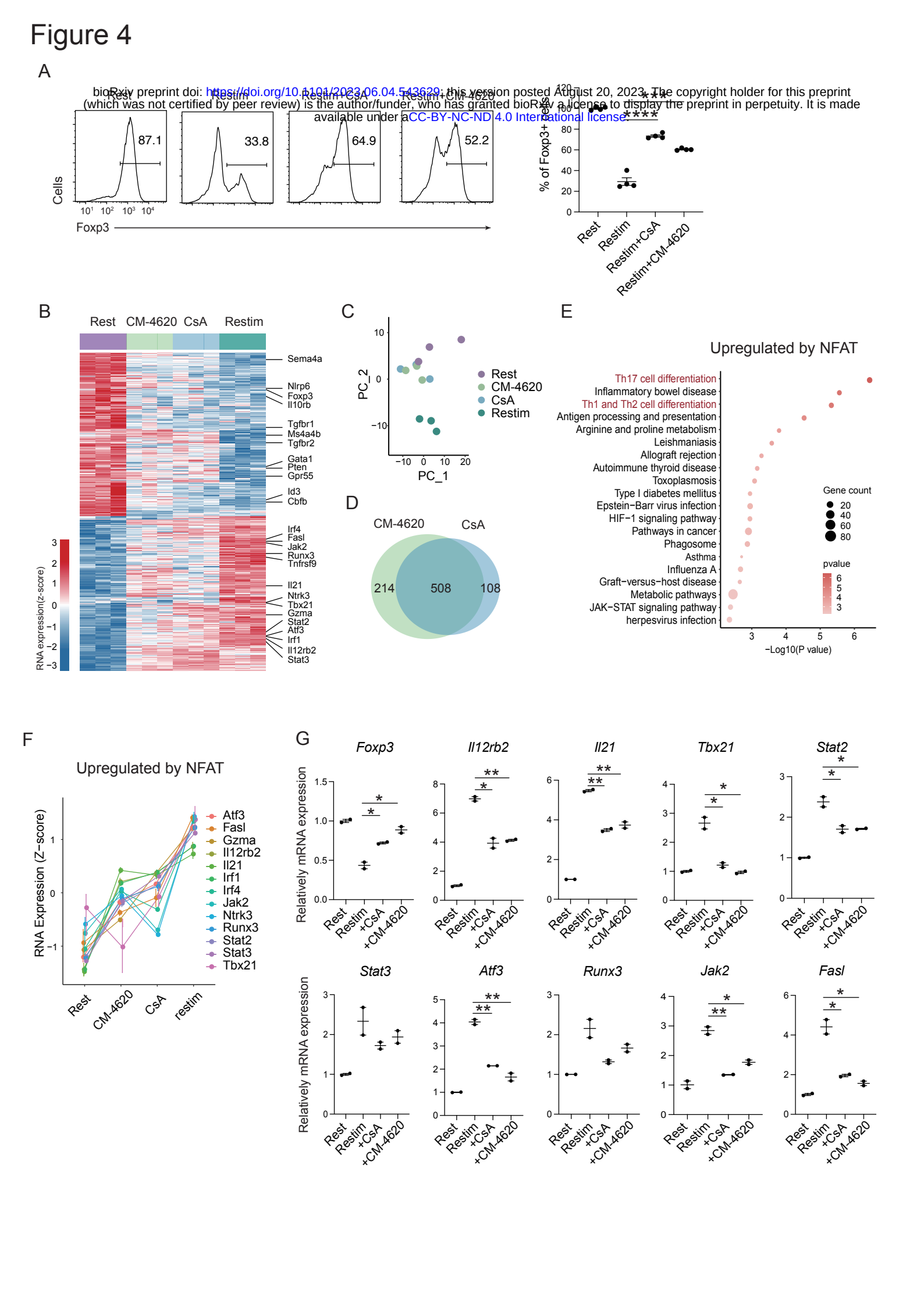

Figure 5

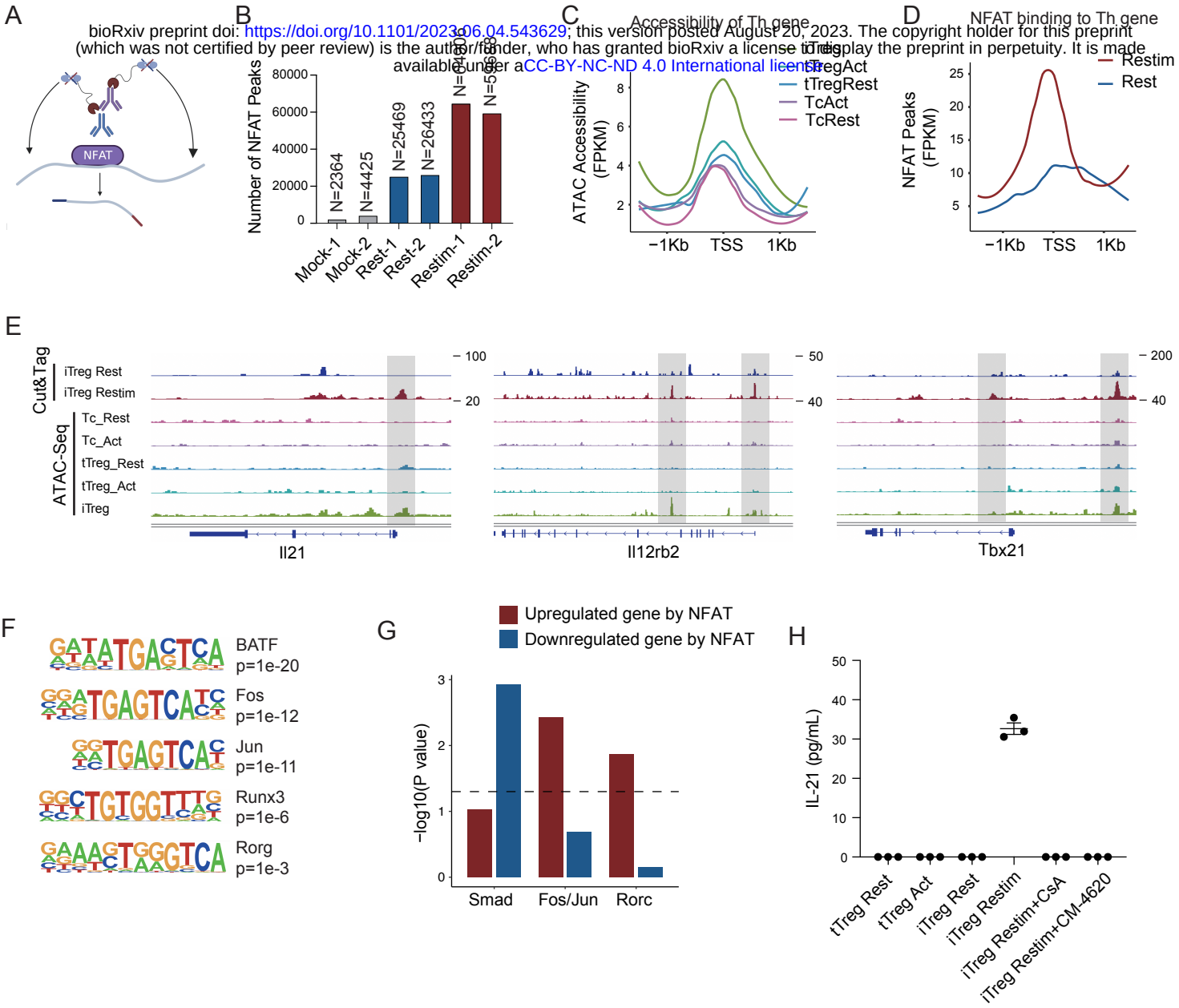

Figure 6

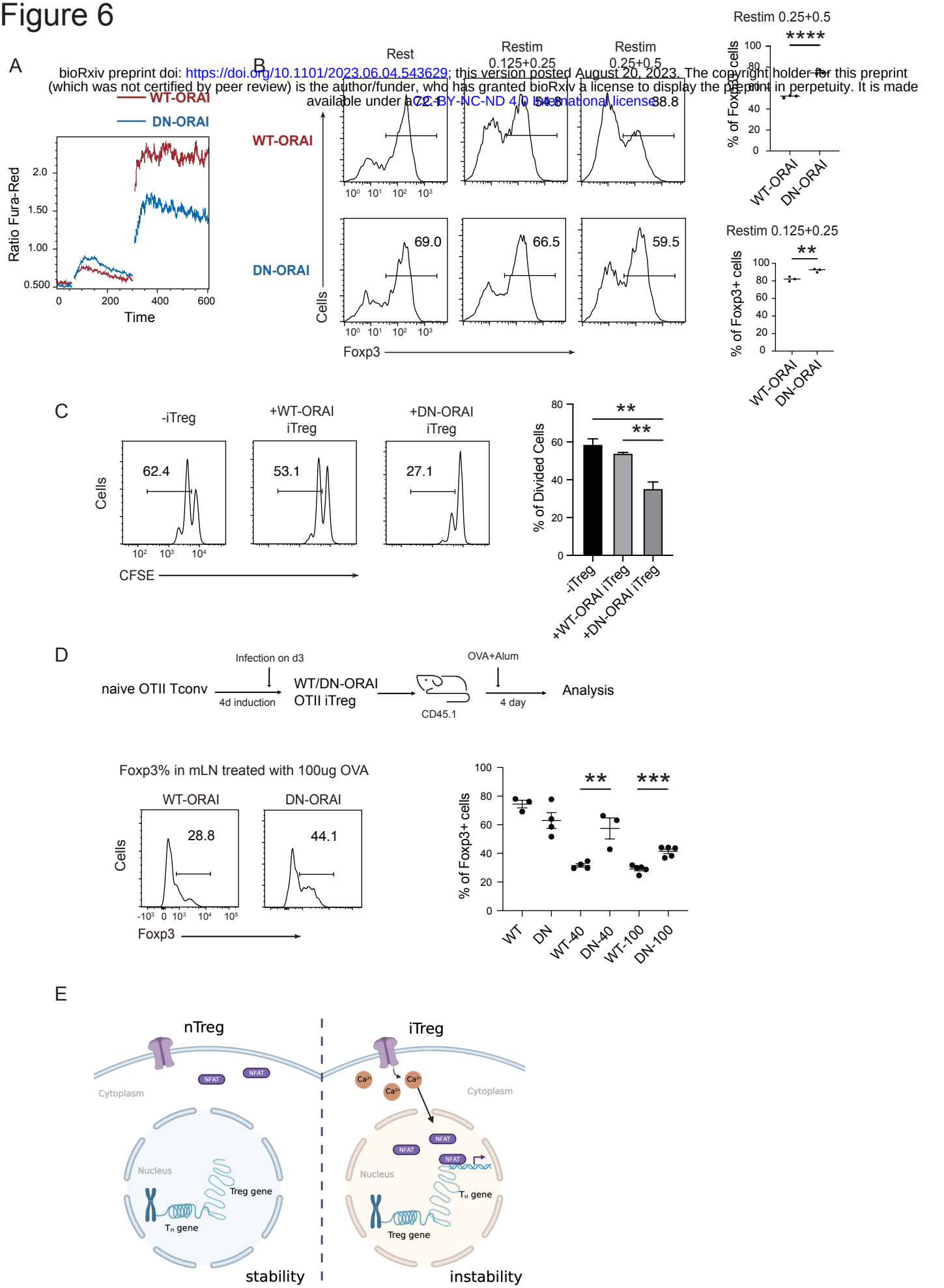

Figure S1

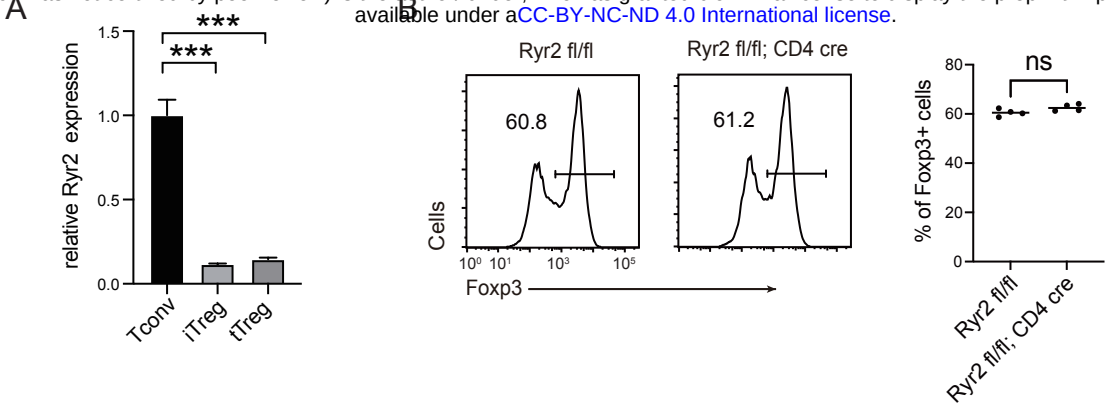

Figure S2

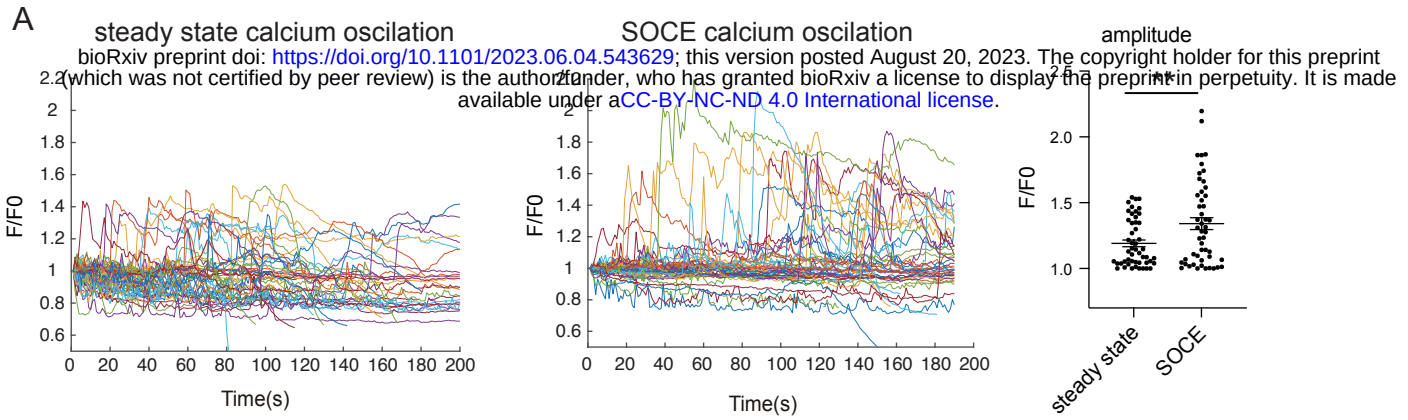

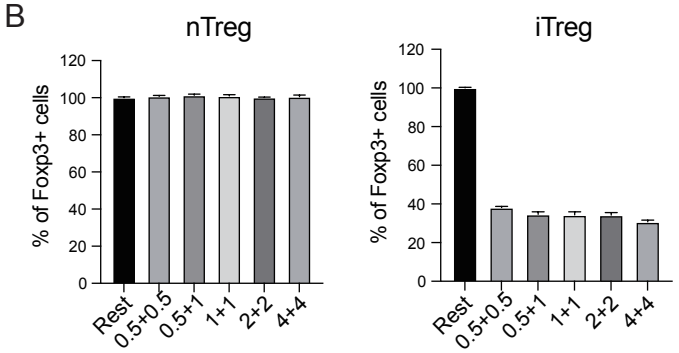

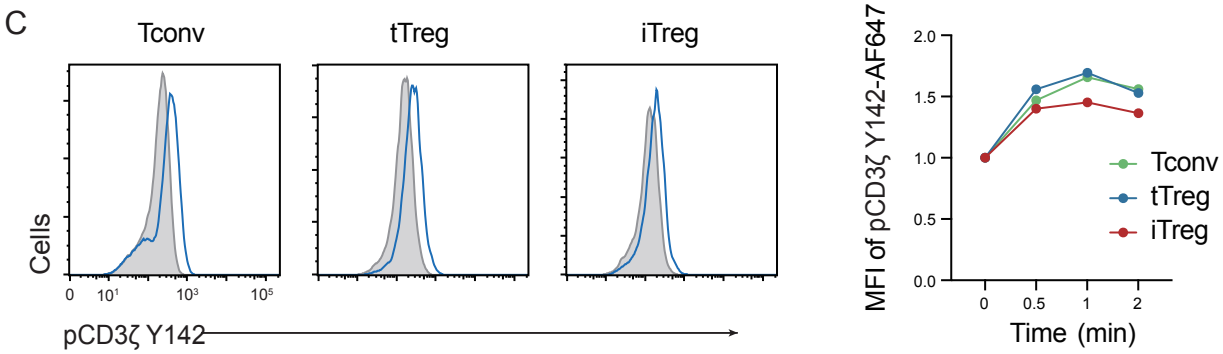

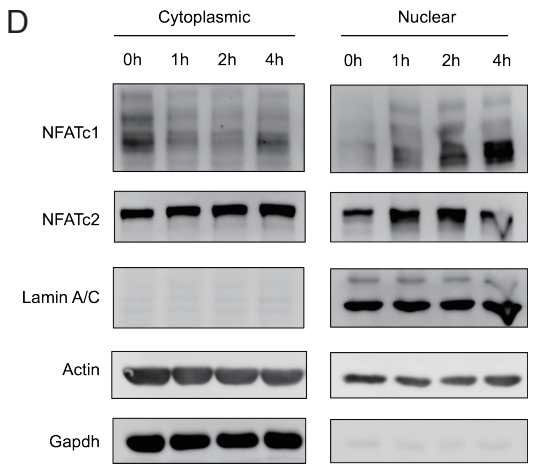

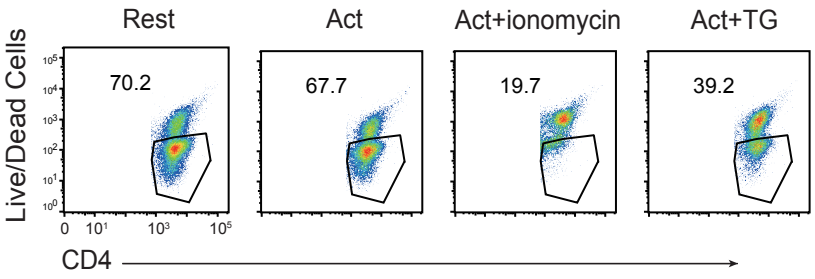

Figure S3

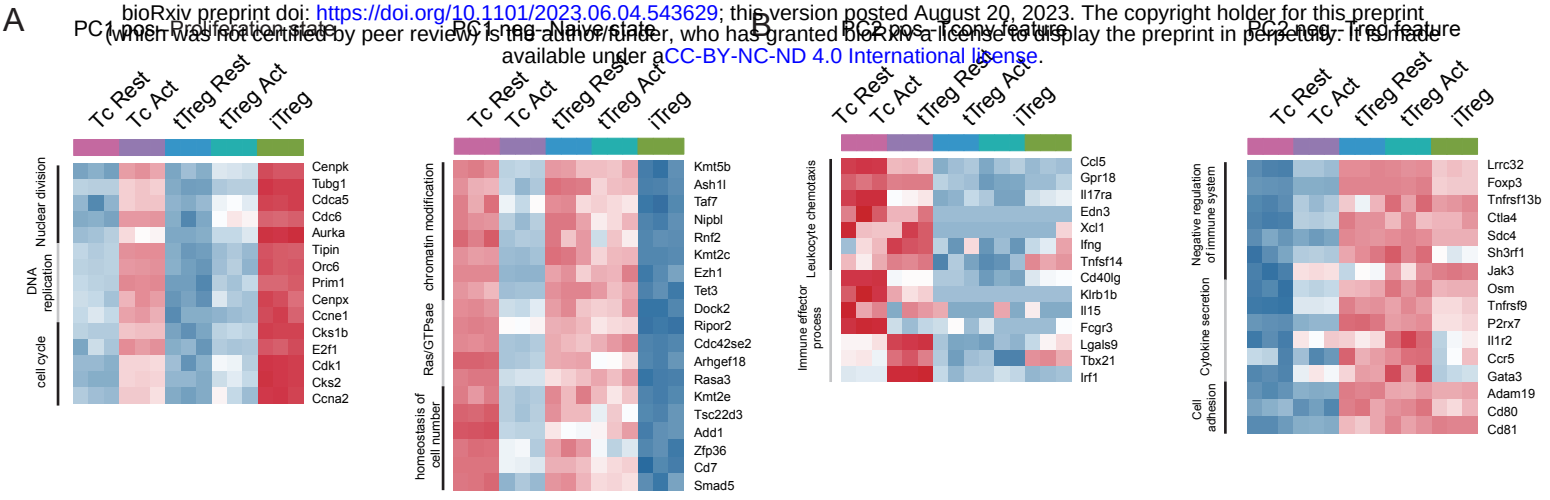

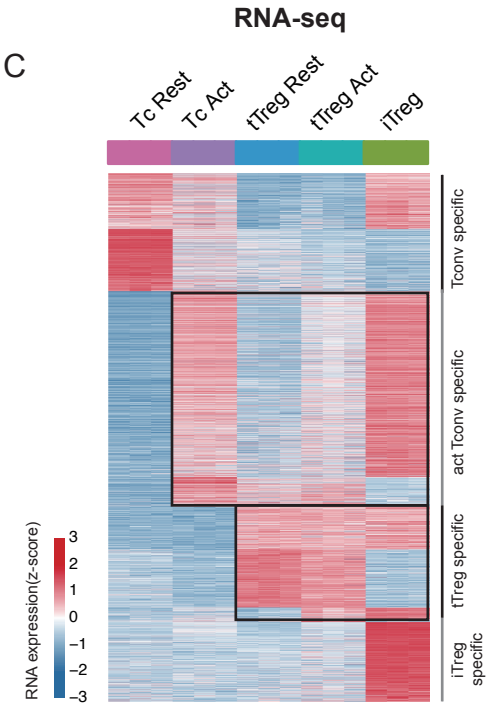

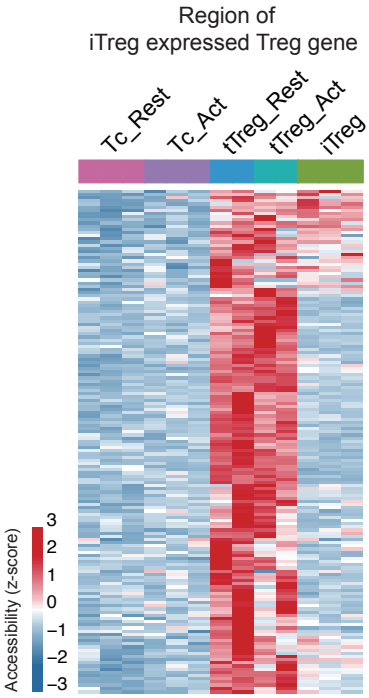

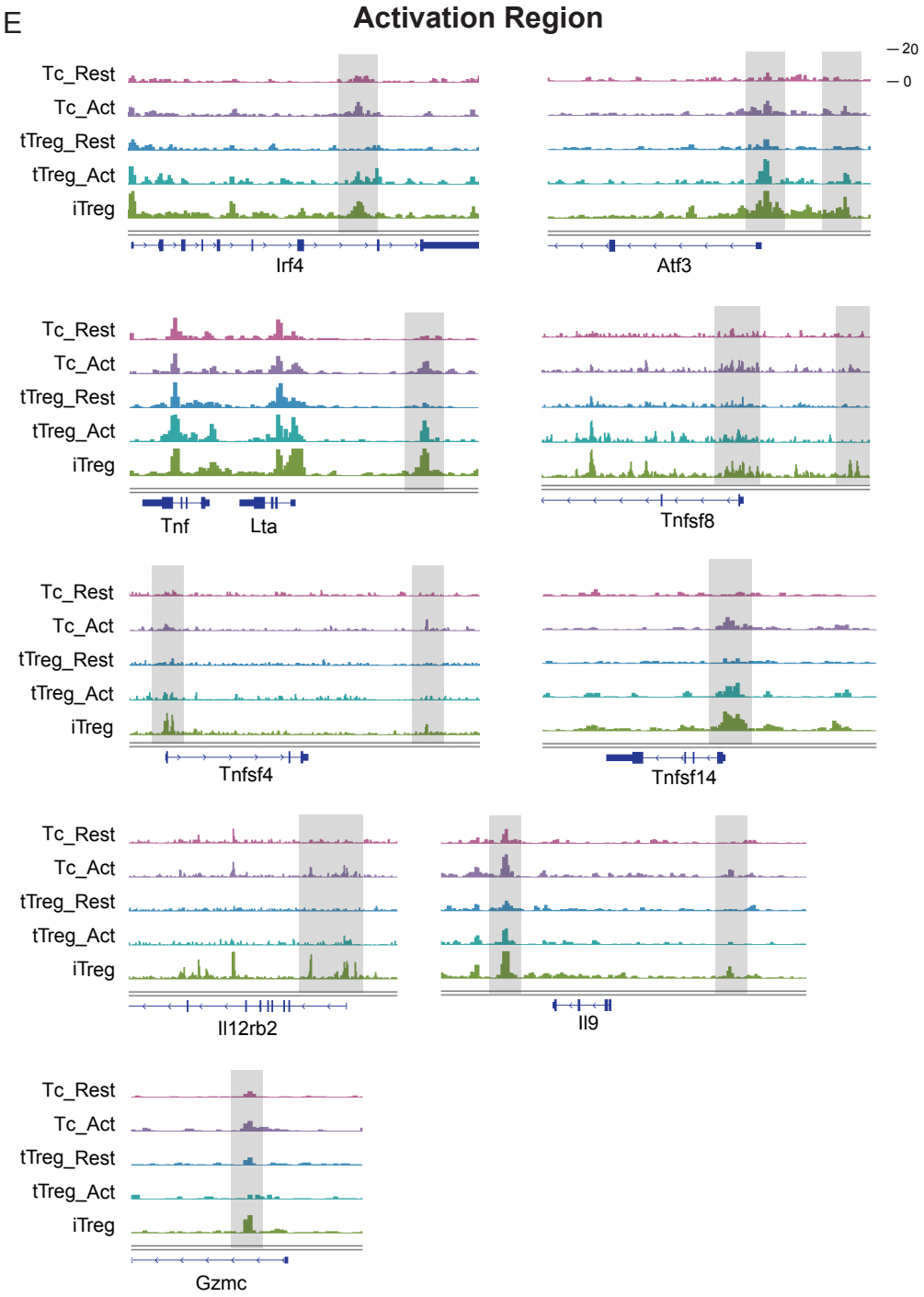

Figure S4

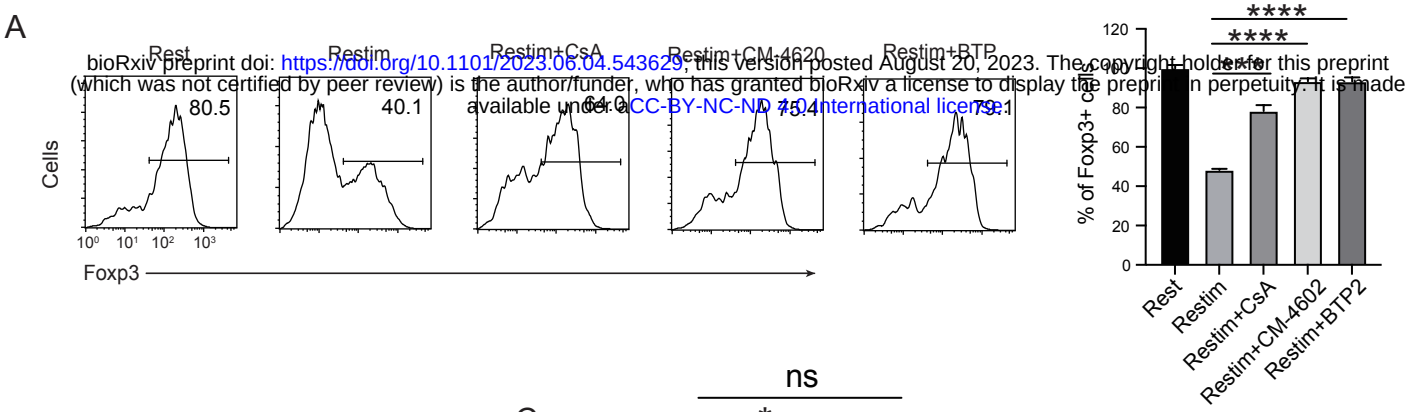

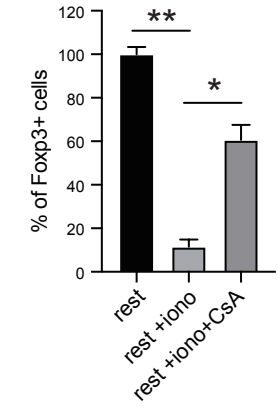

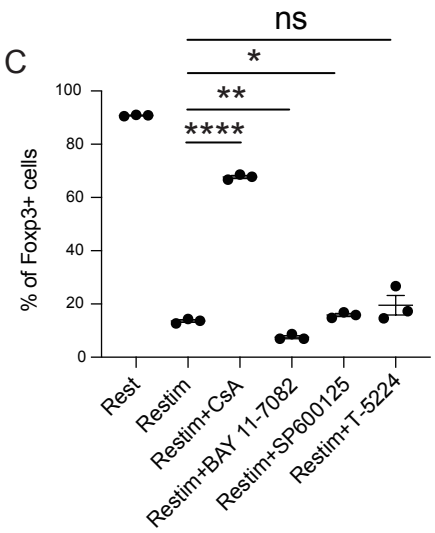

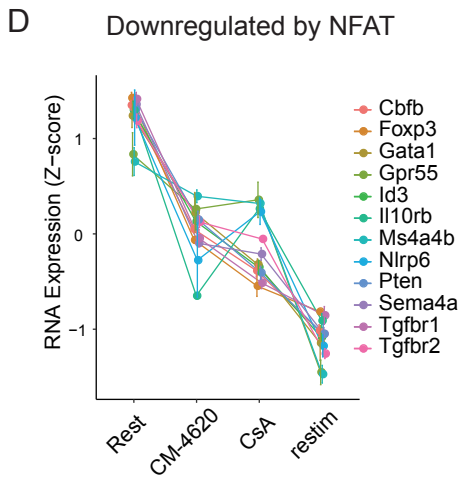

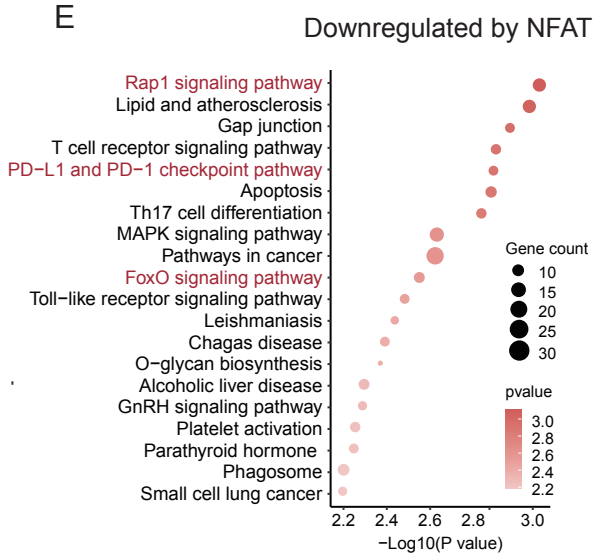

Figure S5

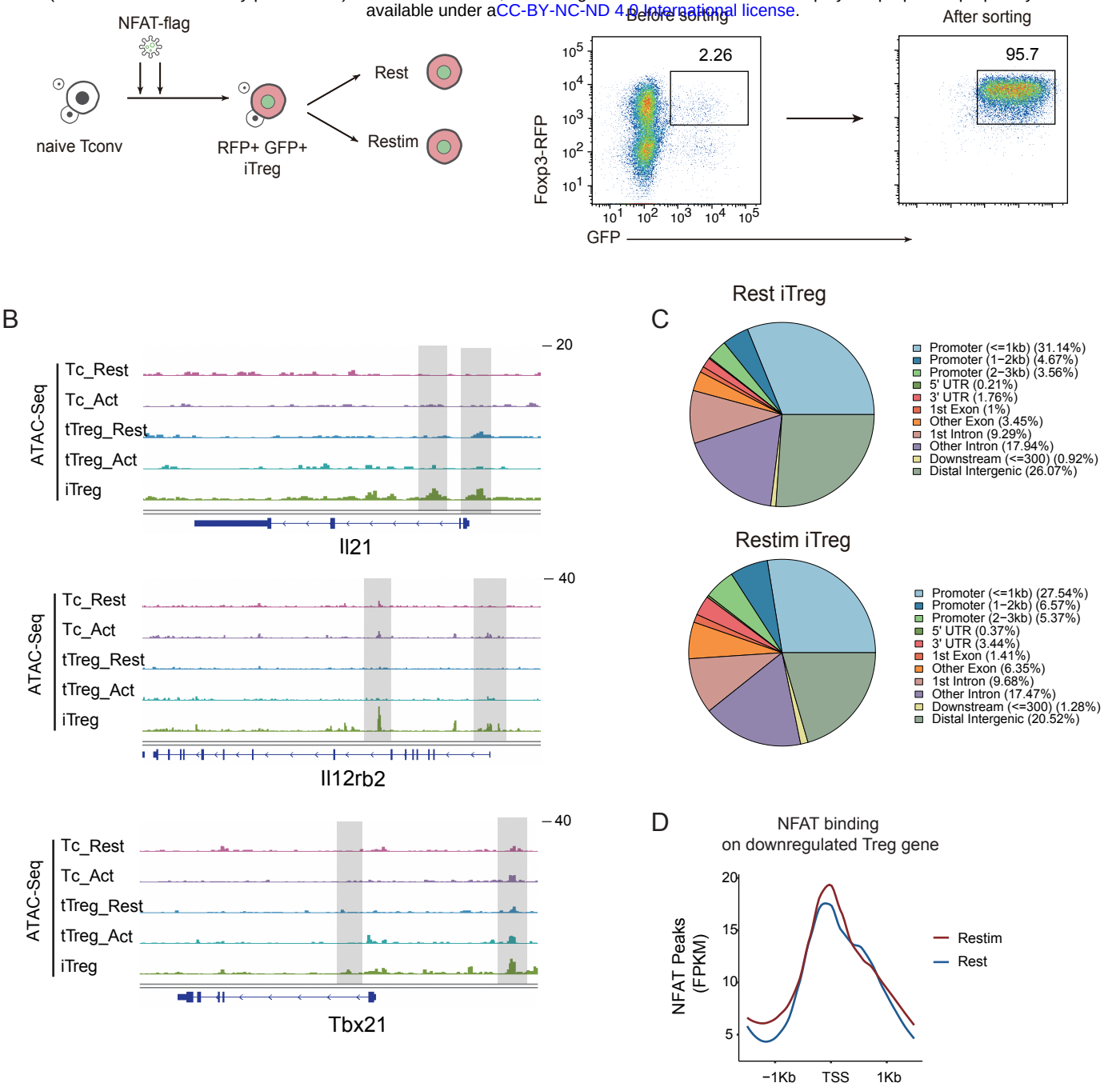

Figure S6

A

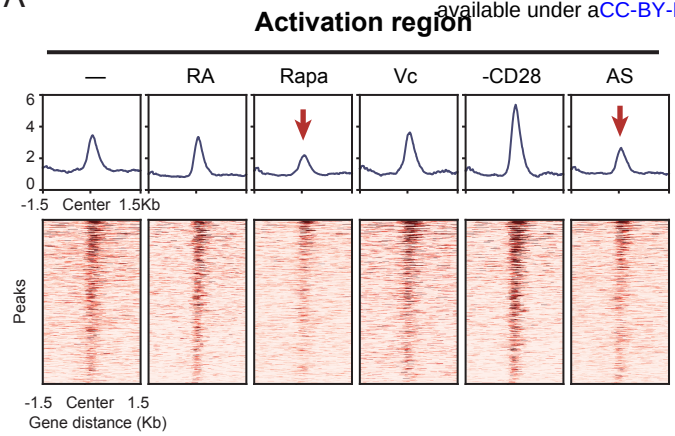

B